Supplementary Information

Precisely synthesized segmented polyurethanes toward block sequence-controlled drug delivery

Yuanqing Song,[a] Chuandong Sun,[a] Chenxu Tian,[a] Hao Ming,[a] Yanjun Wang,[a] Wenkai Liu,[a] Nan He,[a] Xueling He,[b] Mingming Ding,*[a] Jiehua Li,[a] Feng Luo,[a] Hong Tan,*[a] and Qiang Fu[a]

[a] *College of Polymer Science and Engineering, State Key Laboratory of Polymer Materials Engineering, Sichuan University, Chengdu 610065, China*

[b] *Laboratory Animal Center of Sichuan University, Chengdu 610041, China*

* Correspondence to: hongtan@scu.edu.cn; dmmshx@scu.edu.cn

Table of Content Pages

Section 1. Materials and Characterization

Materials

Hydroxy-polyethylene glycol monomethyl ether (mPEG-OH, M_n 2000) and amino-polyethylene glycol monomethyl ether (mPEG-NH_2, M_n 2000) were purchased from Ponsure Biotechnology Co., Ltd. (Shanghai, China). Poly(ε-caprolactone) (PCL, 99%, M_n 2000) was purchased from Daicel Chemical Industries, Ltd. (Japan). PEG and PCL were used after dehydration at 90 °C for 2 h under high vacuum. $_L$-Lysine ethyl ester diisocyanate (LDI, 97%) was attained from Nantong Dahong Chemical Co., Ltd. (Jiangsu, China) and purified by vacuum distillation. Cysamine dihydrochloride (Cysa·2HCl, 97%), ε-caprolactone (ε-CL, 99%), propargylamine (98%), doxorubicin hydrochloride (DOX·HCl, 96%), dicyclohexylcarbodiimide (DCC, 98%), N-hydroxysuccinimide (NHS, 98%), 3-dimethylaminopropylamine (DMAPA, 95%), 1-bromooctane (98%), $(Boc)_2$lysine (95%), 6-aminocaproic acid methyl ester hydrochloride (98%) and tert-butyl 3-phenyl-L-alaninate (Phe-OtBu) were purchased from Chengdu Saibole Technology Co., Ltd (Sichuan, China). Pyrene (95%), the enhanced BCA protein assay kit (P0010, Beyotime Biotechnology), 4',6-diamidino-2-phenylindole (DAPI, 98%) and 3-(4,5-dimethylthiazol-2-yl)-2,5-diphenyltetrazolium bromide (MTT, 98%) were purchased from Chengdu baoke biotechnology Co., Ltd. (Sichuan, China). 2-Azidoethylamine (95%) was synthesized as the previous article reported.[1]

Unless otherwise noted, all chemical reagents were obtained from Chengdu haihong Chemical Reagent Company (Sichuan, China) and used without further purification. Tetrahydrofuran (THF) was dehydrated distilled with metallic sodium and stored in the presence of 4 Å molecular sieves before use.

Characterization

Proton and carbon nuclear magnetic resonance spectroscopy (^{1}H NMR and ^{13}C NMR) was recorded on a Bruker Avance II-600 MHz spectrometer using tetramethylsilane (TMS) as an internal standard and $CDCl_3$ or D_2O as solvents at 25 °C. The sample for ^{1}H-^{1}H NOESY was the micellar aqueous solution with 10% D_2O at the concentration of 10 mg mL^{-1}.

Gel permeation chromatography (GPC) was performed on a Waters 1515-2414 (USA) using Styragel HR 4 Column (7.8 × 300 mm) and Styragel HR 2 Column (7.8 × 300 mm) series system with a Styragel Guard Column (4.6 × 30 mm). Molecular weights are relative to narrow polymethyl methacrylate (PMMA) standards. The mobile phase was N,N-dimethyl-formamide (DMF)/LiBr (0.05 M), and the flow rate was 1.00 mL min^{-1} at 40 °C. The sample concentration was about 3 mg mL^{-1}.

Matrix-assisted laser desorption/ionization time-of-flight mass spectrometry (MALDI-TOF MS) was conducted on an Autoflex MALDI-TOF/TOF (Bruker Daltonic Inc., German) to determine the accurate number-average molecular weights (M_n) in the linear mode and 20 kV acceleration voltage. α-Cyano-4-hydroxycinnamic acid (α-CCA) was used as a matrix to facilitate the deposition of samples in the instrument.

Electrospray ionization mass spectroscopy (ESI-MS) was obtained on a liquid chromatograph-mass spectrometer (Shimadzu, Japan) with methanol as the mobile phase. The compound solution with a concentration of 1×10^{-6} mol mL^{-1} was prepared in methanol, and 0.3 μL solution was injected into the equipment for testing at 25 °C.

Fourier transform infrared (FT-IR) spectra were recorded on a Nicolet iS10 spectrometer (Thermo Electron Corporation, U.S.A) from 4000 to 500 cm^{-1} by a transmission mode. The PUs were dissolved in chloroform (5%) and dropped onto potassium bromide tablets.

Dynamic light scattering (DLS) and **Static light scattering (SLS)** was carried out on a Brookhaven BI-200SM (USA) wide angle laser light scattering with a Spectra Physics Millennia-II diode laser. The micellar samples with a concentration of 100 μg mL^{-1} were purified by passing through a 0.45 μm Millipore filter (PVDF).

The test was conducted with a 532 nm laser at 25 °C, and the detection angle ranged from 30° to 150° with 15° increments between angles. Three repeat measurements of scattered light intensity were taken at each angle and concentration. CONTIN analyses were used for the extraction of hydrodynamic radius (R_H) data from DLS measurements, and radius of gyration (R_G) data were obtained from typical Berry plots of SLS tests. Finally, the characteristic parameter (ρ) was calculated from the ratio of R_G/R_H.

Size and zeta potential of PU assemblies were carried out on Zetasizer Nano ZS instrument (Malvern Instruments Ltd., UK) at 25 °C with a detection angle of 90°. The tests were measured for three times.

Transmission electron microscope (TEM) was acquired on a model H-600-4 (Hitachi, Ltd., Japan) operated at an accelerating voltage of 80 KV. The samples were prepared by depositing the micelles onto the copper grid and negatively staining with 1% (wt/v) phosphotungstic acid for 2 min, the excessive solution was then blotted away and the grid was air-dried before observation.

Section 2. Synthetic and Experimental Protocols

Section 2.1 Synthetic Protocols of Precise Synthetic Platform for PUs through the Liquid-Phase Synthesis Based on the Iterative Diisocyanate Chemistry

2.1.1 Three-segment PUs: the feasibility of monomer connections via the diisocyanate chemistry

Compound 1 (TBA)

Detail descriptions of the synthetic process were provided in the manuscript (experimental methods). It should be noted that the yield is not only affected by the conversion rate of the reaction, but also influenced by the difficulty of purification. For example, the trailing phenomenon of PCL leads to partial product loss and yield decline.

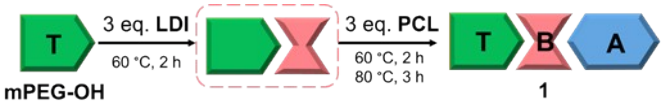

Scheme S1. The synthetic flow diagram of compound **1** (TBA): from mPEG with mono hydroxyl group (T), connecting the dihydroxyl monomer (PCL, A, a typical macromolecular diol) via the diisocyanate segment (LDI, B).

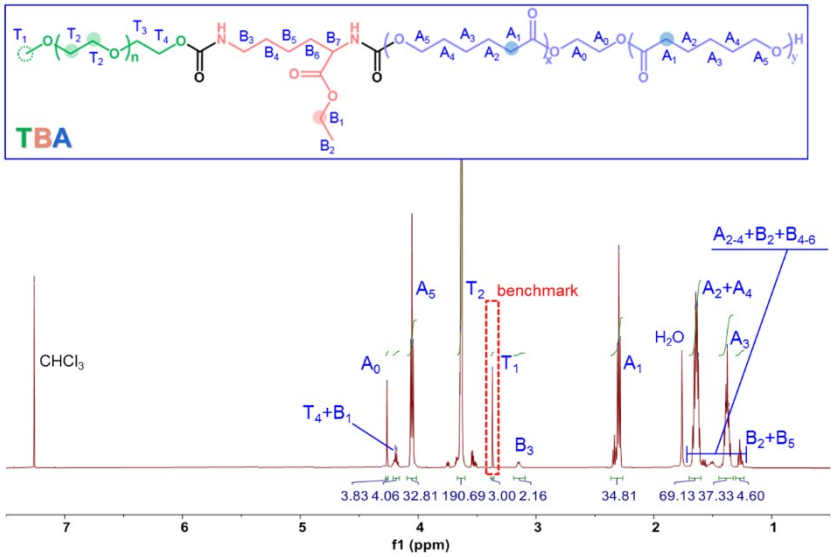

Figure S1. ^{1}H NMR spectrum ($CDCl_3$, 600 MHz, δ 7.50~0.50 ppm) of compound **1** (TBA).

Note: The accurate compositions were determined and number-average molecular weights were calculated according to the integration areas of mPEG-OH ($C\underline{H_3}$-O-, 3.38 ppm; -O-$C\underline{H_2}C\underline{H_2}$-O-, 3.64 ppm), LDI ($CH_3C\underline{H_2}$-O-, 4.20 ppm), PCL (-O-$C\underline{H_2}C\underline{H_2}$-O-, 4.27 ppm; -$CH_2C\underline{H_2}$-CO-, 2.32 ppm) and Cysa (-$CH_2C\underline{H_2}$-S-S-, 2.82 ppm) with mPEG ($C\underline{H_3}$-O-, 3.38 ppm) as the benchmark.

[M] (x) refers to the accurate molecular weight of micromolecular segment x (e.g. LDI), and I_y means the integral area of y proton for each macromers (e.g. mPEG-OH and PCL). Statistically number-average molecular weight (M_n) of compound **1** were calculated based on the composition of target chain and the molecular weights of all segments:

M_n (**1**, TBA) = M_n (T) + [M] (B) + M_n (A) = (32 + 44 × I_b/4) + (226) + (114 × I_g/2 + 62) ≈ 4,400 g mol^{-1}

Compound 2 (T'BC)

Detail descriptions of the synthetic process were provided in the manuscript (experimental methods). Although the high reaction conversion was verified by TLC, the yield was greatly decreased by the difficulty of the purification, because T'BC and T' possessed the similar structure and the same terminal group.

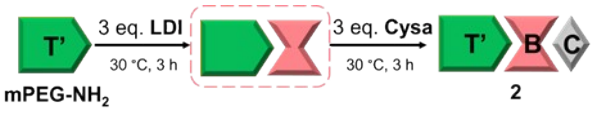

Scheme S2. The synthetic flow diagram of **2** (T'BC): from mPEG with mono amino group (T'), connecting the diamino monomer (Cysa, C, a typical small molecular diamine) via the diisocyanate segment (LDI, B).

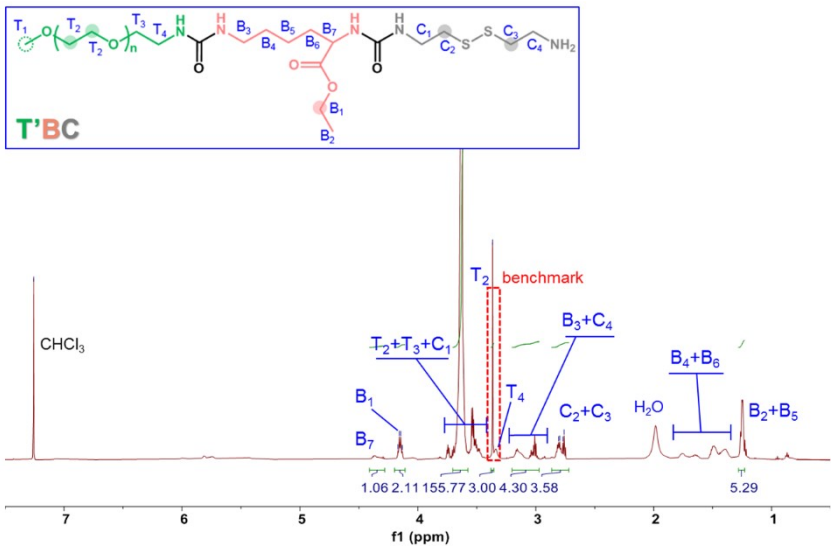

Figure S2. ^{1}H NMR spectrum ($CDCl_3$, 600 MHz, δ 7.50~0.50 ppm) of compound **2** (T'BC).

Note: The accurate compositions were determined and number-average molecular weights were calculated according to the integration areas of mPEG-NH_2 (CH_3-O-, 3.38 ppm; -O-CH_2CH_2-O-, 3.64 ppm), LDI (CH_3CH_2-O-, 4.20 ppm) and Cysa (-CH_2CH_2-S-S-, 2.82 ppm) with mPEG' (CH_3-O-, 3.38 ppm) as the benchmark.

Statistically number-average molecular weight (M_n) of compound **2** were calculated based on the composition of target chain and the molecular weights of all segments:

M_n (**2**, T'BC) = M_n (T') + [M] (B) + [M] (C) = (31 + 44 × I_b/4) + (226) + (152) ≈ 2,200 g mol^{-1}

2.1.2 Five-segment PUs: linear growth via the iterative diisocyanate procedures

Compound 3 (TBABC)

Detail descriptions of the synthetic process were provided in the manuscript (experimental methods).

Scheme S3. The synthetic flow diagram of **3** (TBABC) via the iterative diisocyanate chemistry: from mPEG with mono hydroxyl group (T), firstly connecting the dihydroxyl monomer (A), then connecting the diamino monomer (C).

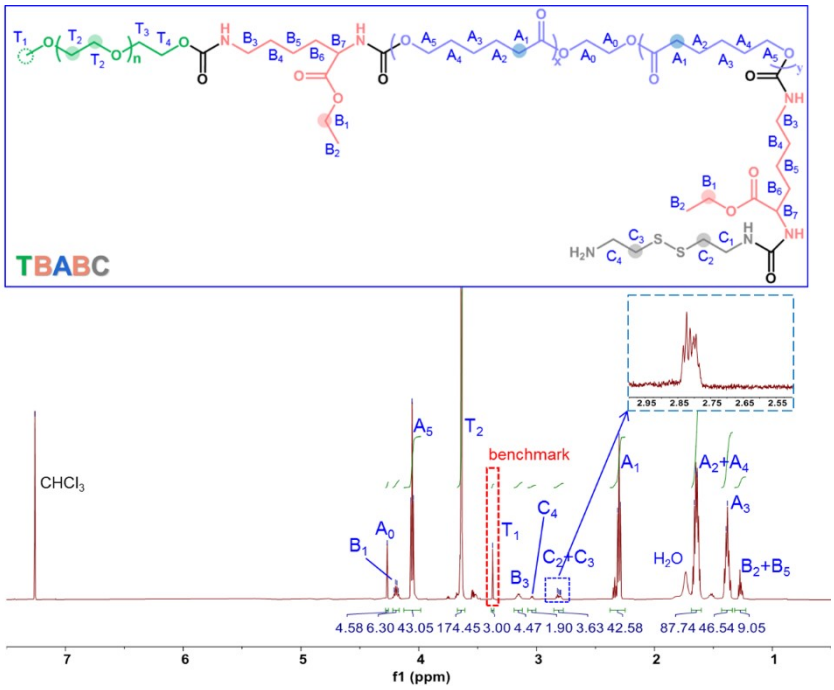

Figure S3. ^{1}H NMR spectrum ($CDCl_3$, 600 MHz, δ 7.50~0.50 ppm) of compound **3** (TBABC).

Note: Calculated M_n of compound **3** based on the composition of target chain and the molecular weights of all segments:

M_n (**3**, TBABC) = M_n (T) + 2 × [M] (B) + M_n (A) + [M] (C) = (32 + 44 × I_b/4) + (2 × 226) + (114 × I_g/2 + 62) + (152) ≈ 5,000 g mol^{-1}

Compound 4 (T'BCBA)

The synthetic diagram of **4** was shown in Scheme S4. In brief, **2** (T'BC, 1 mmol) and LDI (B, 3 mmol) dissolved in dehydrated THF were reacted at 30 °C for 3 h under nitrogen environment. After T'BC was almost converted, the reaction solution was added into anhydrous diethyl ether, and the solution was refrigerated at -24 °C for 1 h. Then, the purified intermediate product (T'BCB) was quickly collected by suction filtration and washed twice with diethyl ether. Then the reaction of dried T'BCB and PCL (A, 3 mmol) with organic bismuth was performed at 60 °C for 2 h, and at 80 °C for another 3 h under nitrogen environment. Finally, the purification process of compound **4** (T'BCBA) was similar to that of **1** (TBA). The target collecting ratio was about 35:1 (chloroform/methanol, v/v) to give the product as white solid (~30% yield).

^{1}H NMR (600 MHz, $CDCl_3$, ppm): δ = 4.27 (t, 4H, A), 4.20 (q, 4H, B), 4.06 (t, 38H, A), 3.64 (t, 163H, T'), 3.38 (s, 3H, T'), 3.15 (d, 4H, B), 2.81 (m, 4H, C), 2.32 (t, 42H, A), 1.65 (m, 83H, A), 1.38 (m, 46H, A), 1.27 (m, 9H, B).

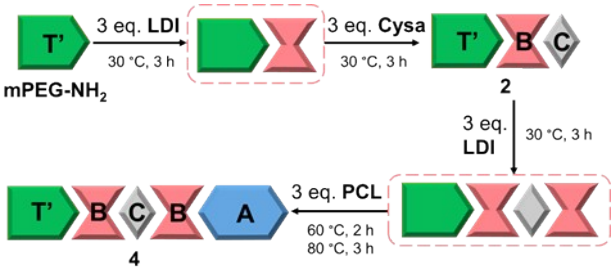

Scheme S4. The synthetic flow diagram of **4** (T'BCBA) via the iterative diisocyanate chemistry: from mPEG with mono amino group (T'), firstly connecting the diamino monomer (C), then connecting the dihydroxyl monomer (A).

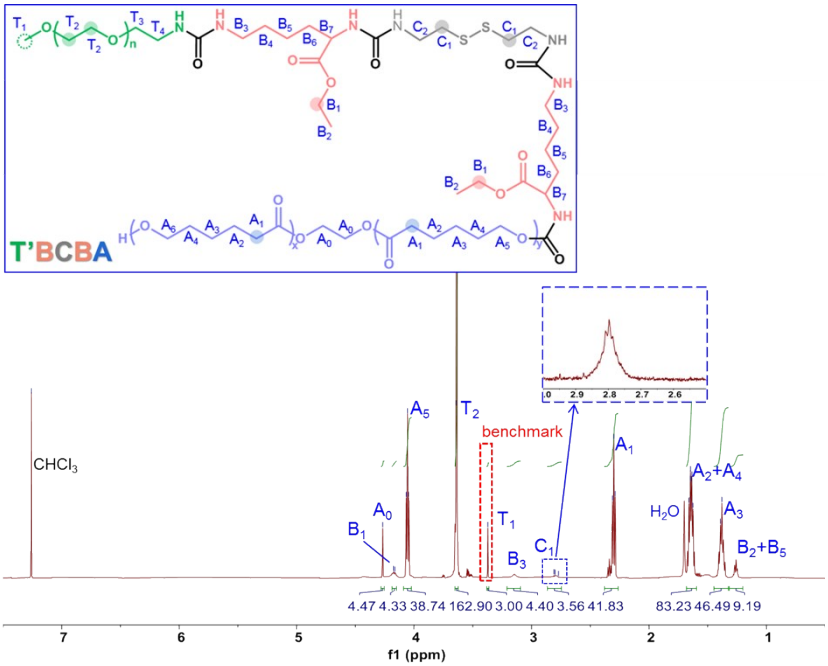

Figure S4. ^{1}H NMR spectrum ($CDCl_3$, 600 MHz, δ 7.50~0.50 ppm) of compound **4** (T'BCBA).

Note: Calculated M_n of compound **4** based on the composition of target chain and the molecular weights of all segments:

M_n (**4**, T'BCBA) = M_n (T') + 2 × [M] (B) + [M] (C) + M_n (A) = (31 + 44 × I_b/4) + (2 × 226) + (152) + (114 × I_g/2 + 62) ≈ 4,900 g mol^{-1}

Compound 5 (TBABA)

The synthetic diagram of **5** was shown in Scheme S5. Briefly, **1** (TBA, 1 mmol) and LDI (B, 5 mmol) with organic bismuth were added into a three-necked flask for 3 h of reaction at 60 °C under nitrogen environment. After TBA was almost converted, anhydrous THF/diethyl ether (1:1, v/v) were used for refrigeration at -24 °C for 2 h. The purified intermediate product (TBAB) was quickly collected by suction filtration and washed twice with diethyl ether. Then the reaction of dried TBAB and PCL (A, 5 mmol) with organic bismuth was carried out at 60

°C for 2 h, and at 80 °C for another 3 h under nitrogen environment. Finally, the similar purification process was conducted for compound **5** (TBABA), and the target collecting ratio was about 45:1 (v/v) to give the product as white solid (~21% yield).

^{1}H NMR (600 MHz, $CDCl_3$, ppm): δ = 4.27 (t, 7H, A), 4.20 (m, 6H, B), 4.06 (t, 66H, A), 3.64 (t, 179H, T), 3.38 (s, 3H, T), 3.15 (d, 5H, B), 2.32 (t, 68H, A), 1.65 (m, 138H, A), 1.38 (m, 72H, A), 1.27 (m, 10H, B).

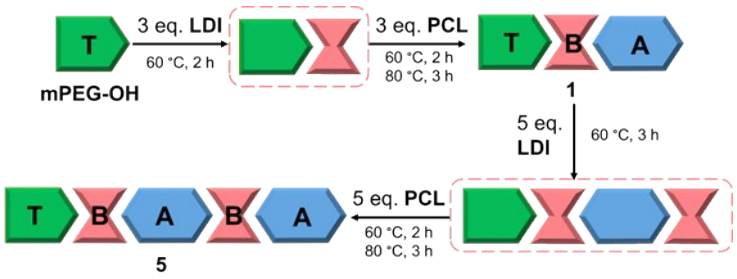

Scheme S5. The synthetic flow diagram of **5** (TBABA) via the iterative diisocyanate chemistry: the short chain used to prepare the macromolecule below.

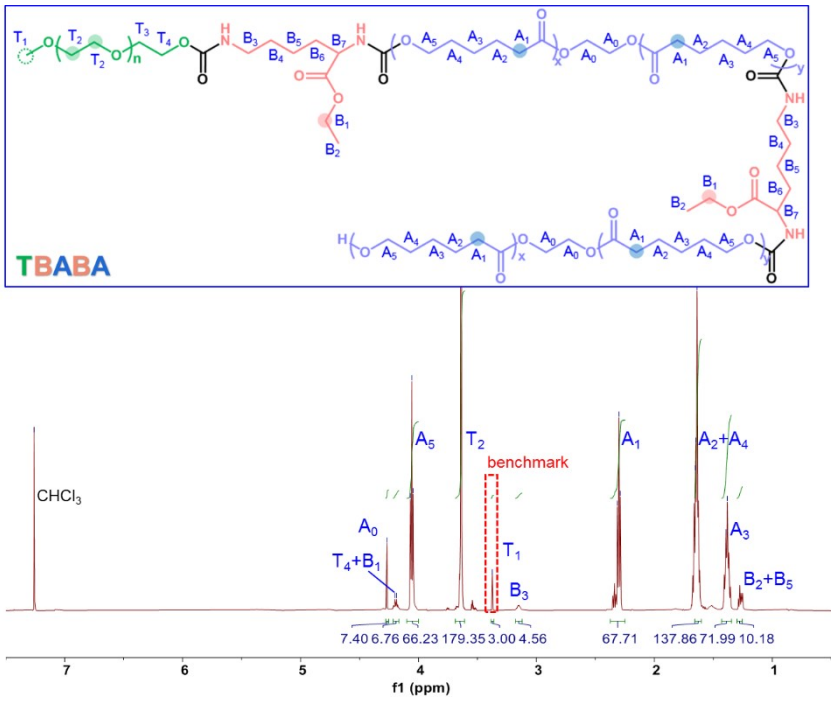

Figure S5. ^{1}H NMR spectrum ($CDCl_3$, 600 MHz, δ 7.50~0.50 ppm) of compound **5** (TBABA).

Note: Calculated M_n of compound **5** based on the composition of target chain and the molecular weights of all segments:

M_n (**5**, TBABA) = M_n (T) + 2 × [M] (B) + M_n (A) = (32 + 44 × I_b/4) + (2 × 226) + (114 × I_g/2 + 2 × 62) ≈ 6,500 g mol^{-1}

2.1.3 Convergent strategies: rapid growth of molecular weights

Compound 6 (T'BCBABT)

Detail descriptions of the synthetic process were provided in the manuscript (experimental methods).

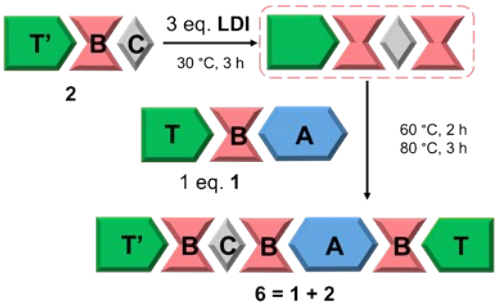

Scheme S6. The synthetic flow diagram of **6** (T'BCBABT): the convergent strategy based on the diisocyanate chemistry to achieve the rapid growth of molecular weight.

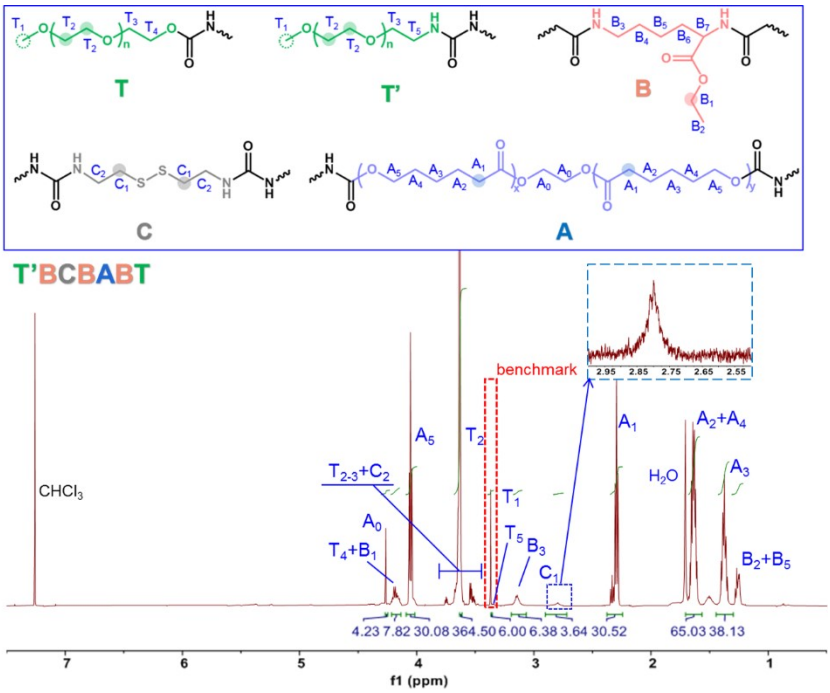

Figure S6. ^{1}H NMR spectrum ($CDCl_3$, 600 MHz, δ 7.50~0.50 ppm) of compound **6** (T'BCBABT).

Note: Calculated M_n of compound **6** based on the composition of target chain and the molecular weights of all segments:

M_n (**6**, T'BCBABT) = M_n (T') + M_n (T) + 3 × [M] (B) + [M] (C) + M_n (A) = (31 + 32 + 44 × I_b/4) + (3 × 226) + (152) + (114 × I_g/2 + 62) ≈ 6,700 g mol^{-1}

Compound 7 (TBABABC'-C''BABABT)

The convergent strategy was based on the click chemistry: copper-catalyzed azido-alkyne cycloaddition reaction (CuAAC)[1]. Hence, two steps were included: the synthesis of two clickable chains (a), and the CuAAC to achieve the efficient connection (b).

a. mPEG-LDI-PCL-LDI-PCL-LDI-propargylamine/2-azidoethylamine (TBABABC' / TBABABC'')

As shown in Scheme S7a, the synthetic process of TBABABC' / TBABABC'' was similar to that of **3** (T'BABC), where C' and C'' refer to the clickable monomers of propargylamine and 2-azidoethylamine, respectively. Higher feed ratio was adjusted to guarantee the reaction conversion. Without column chromatography, the final products were purified only by THF/diethyl ether (1:2, v/v) refrigeration at -24 °C for 3

h.

b. TBABABC'-C''BABABT

The reaction condition was shown in Scheme S7b. With the catalysis of NaVc (2 mmol) and $CuSO_4 \cdot 5H_2O$ (1 mmol), the purified TBABABC' (1 mmol) and TBABABC'' (1 mmol) dissolved in THF/H_2O (2:1, v/v) were reacted at 30 °C for 12 h under nitrogen atmosphere. After dialysis to remove the catalysts, the product was obtained through column chromatography. The target receiving ratio for compound **7** (TBABABC'-C''BABABT) was about 40:1 (chloroform/methanol, v/v), and the product was white solid after vacuum drying (~70%, yield). Besides, precipitation fractionation was further applied in the purification process if necessary.

^{1}H NMR (600 MHz, $CDCl_3$, ppm): δ = 4.27 (t, 16H, A), 4.20 (m, 16H, B+T), 4.06 (t, 130H, A), 3.64 (t, 364H, T), 3.38 (s, 6H, T), 3.15 (d, 13H, B), 2.32 (t, 138H, A), 1.65 (m, 281H, A), 1.38 (m, 151H, A), 1.27 (m, 31H, B). ^{13}C NMR (600 MHz, $CDCl_3$, ppm): δ = 173.2, 156.8, 72.8, 71.8, 70.3, 63.9, 62.2, 60.7, 58.5, 54.3, 40.0, 34.0, 33.7, 32.6, 30.8, 29.4, 28.9, 28.3, 25.4, 24.6, 23.2, 14.5.

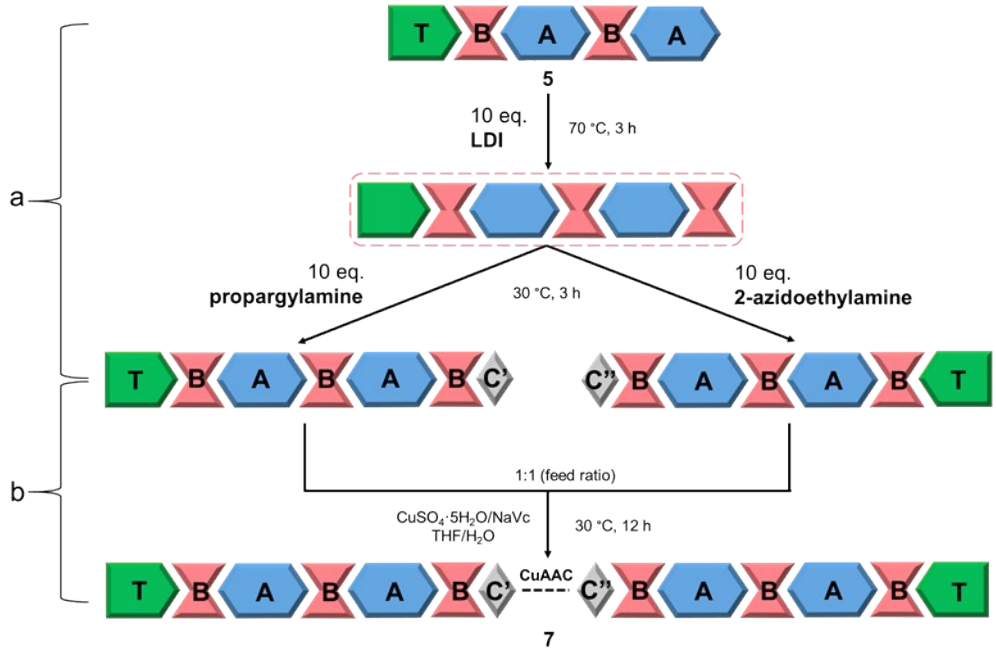

Scheme S7. The synthetic flow diagram of **7** (TBABABC'-C''BABABT): the convergent strategy based on the click chemistry (CuAAC) to synthesize macromolecule with high molecular weight.

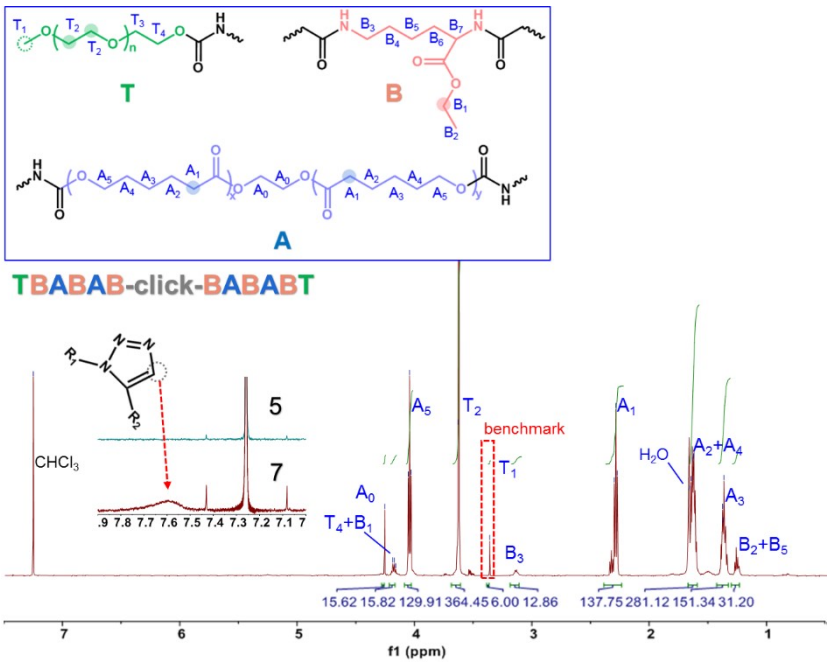

Figure S7. ^{1}H NMR spectrum ($CDCl_3$, 600 MHz, δ 7.50~0.50 ppm) of compound **7** (TBABABC'-C''BABABT). Insert: enlarged stacked ^{1}H NMR spectra (δ 8.0~7.0 ppm) of compounds **5** and **7**.

Note: Calculated M_n of compound **7** based on the composition of target chain and the molecular weights of all segments:

M_n (**7**, TBABABC'-C''BABABT) = 2 × M_n (T) + 6 × [M] (B) + 4 × M_n (A) + [M] (C') + [M] (C'') = (2 × 32 + 44 × I_b/4) + (6 × 226) + (114 × I_g/2 + 4 × 62) + (83) + (86) ≈ 13,700 g mol^{-1}

Section 2.2 Synthetic Protocols of Sequence-Controlled Multifunctional PUs Based on the Established Precise Synthetic Platform above

2.2.1 Synthesis of structural and functional segments

Model functional segment: quaternary ammonium salt with single-carbon chain (Q)[2]

The reaction pathway was shown in Scheme S8. Briefly, $(Boc)_2$lysine (3 mmol) and N-hydroxysuccinimide (NHS, 3.6 mmol) were dissolved in dichloromethane (DCM, 20 mL), then dicyclohexylcarbodiimide (DCC, 3.3 mmol) was added stepwise with stirring in an ice-salt bath to create an active-ester intermediate with carboxylic group of $(Boc)_2$lysine. After 2 h at room temperature, 3-dimethylaminopropylamine (DMAPA, 3.3 mmol) dissolved in DCM (5 mL) was added into the mixture, and the reaction proceeded overnight at room temperature. After the completion of the reaction, the reaction mixture was condensed under reduced pressure. The crude product was dissolved in ethyl acetate (EtOAc, 50 mL) to remove the insoluable impurities, and then saturated salt water was added. After the water layer was extracted with EtOAc for several time, the combined EtOAc solution was concentrated under reduced pressure. Subsequently, the product and 1-bromooctane (3.6 mmol) with $NaHCO_3$ (0.6 mmol) were dissolved in 2-propanol (100 mL), then the mixture was refluxed with stirring at 83 °C for 36 h. After the reaction was finished, the solvent was removed by rotary evaporator, and the product was dissolved in 60 mL of EtOAc saturated with hydrogen chloride for 1 h of reaction in an ice bath and another 4 h of reaction at room temperature. Finally, the crude product was purified by silica gel column chromatography (chloroform/methanol = 10:1 to 1:1, v/v) to give cationic segment (Q) as yellow solid with high purity (56% yield).

^{1}H NMR (600 MHz, CD_3OD, ppm): δ = 3.91 (t, 1H), 3.40-3.20 (m, 6H), 3.01 (s, 6H), 2.98 (t, 2H), 1.97 (m, 2H), 1.86 (m, 2H), 1.67 (m, 4H), 1.41 (m, 2H), 1.40-1.20 (m, 10H), 0.88 (t, 3H). MS (ESI, m/z): calculated for

$C_{19}H_{43}N_4OBr$ 423.48, observed $[M-Br]^+$ 343.13.

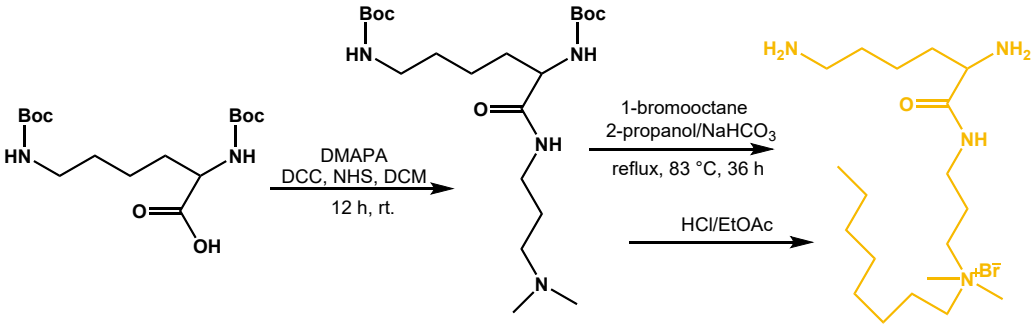

Scheme S8. The synthetic route of quaternary ammonium salt with single-carbon chain (Q).

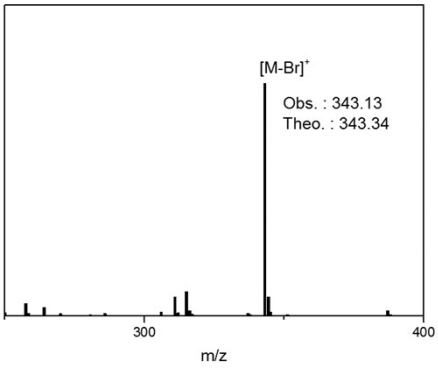

Figure S8. ESI-MS spectrum of lysine-derived quaternary ammonium salt with single-alkyl chain (Q).

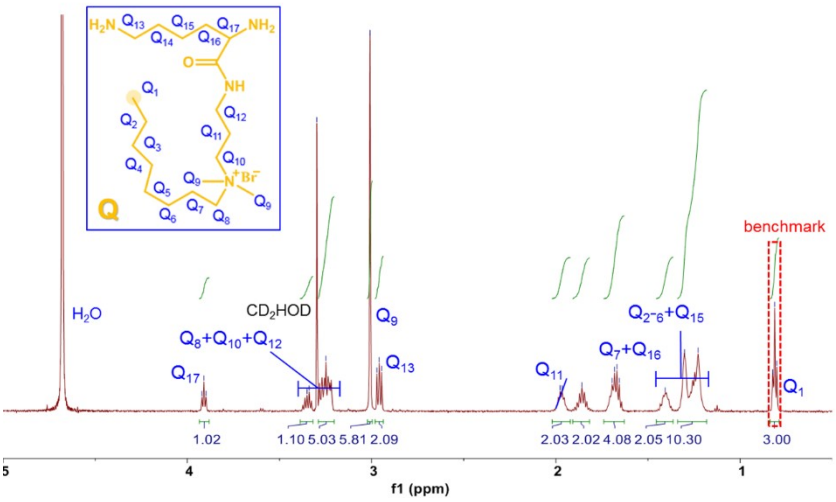

Figure S9. ^{1}H NMR spectrum (CD_3OD, 600 MHz, δ 5.00~0.50 ppm) of quaternary ammonium salt with single-alkyl chain (Q).

Model functional segment: tripeptide with active carboxyl group (K)[3]

The synthetic route was shown in Scheme S9. The active-ester intermediate of $(Boc)_2$lysine was obtained as described above. A solution of 6-aminocaproic acid methyl ester hydrochloride (AAME, 3.3 mmol) in DCM (5 mL) containing triethylamine (TEA, 3.6 mmol) was added into the intermediate solution, and then the reaction

proceeded overnight at room temperature. After the reaction was complete, the reaction mixture was condensed under reduced pressure, then the crude product dissolved in EtOAc (50 mL) was orderly washed with 3M hydrochloric acid, saturated sodium bicarbonate solution, saturated salt water and deionized water. Finally, the collecting product after rotary evaporator was hydrolyzed in methanol (20 mL) containing 4 M sodium hydroxide for 2 h, and then the solution pH value was adjusted between 6-7 to achieve the dipeptide containing carboxylic group. The following synthesis processes of tripeptide were performed according to the same procedures described above. The product was dissolved in 60 mL of EtOAc saturated with hydrogen chloride for 1 h of reaction in an ice bath and another 4 h of reaction at room temperature. The solution was concentrated under reduced pressure and hydrogen chloride was neutralized with saturated sodium bicarbonate solution to attain the active carboxyl group. The crude product was purified by column chromatography (chloroform/methanol = 10:1 to 5:3, v/v) to give anion segment (K) as yellow solid (74% yield).

^{1}H NMR (D_2O, 600 MHz, ppm): δ = 7.30-7.10 (m, 5H), 4.40 (dd, 1H), 3.27 (t, 1H), 3.20-2.80 (m, 6H), 2.09 (m, 2H), 1.56 (m, 4H), 1.35 (m, 6H), 1.02 (m, 2H). MS (ESI, m/z): calculated for $C_{21}H_{34}N_4O_4$ 406.53, observed $[M+H]^+$ 407.39.

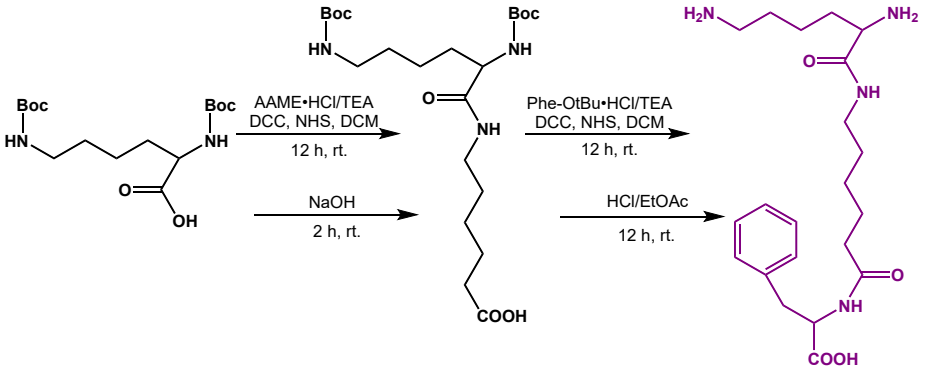

Scheme S9. The synthetic route of tripeptide with active carboxyl group (K).

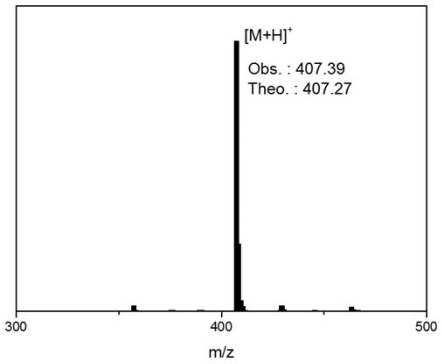

Figure S10. ESI-MS spectrum of lysine-derived tripeptide with active carboxyl group (K).

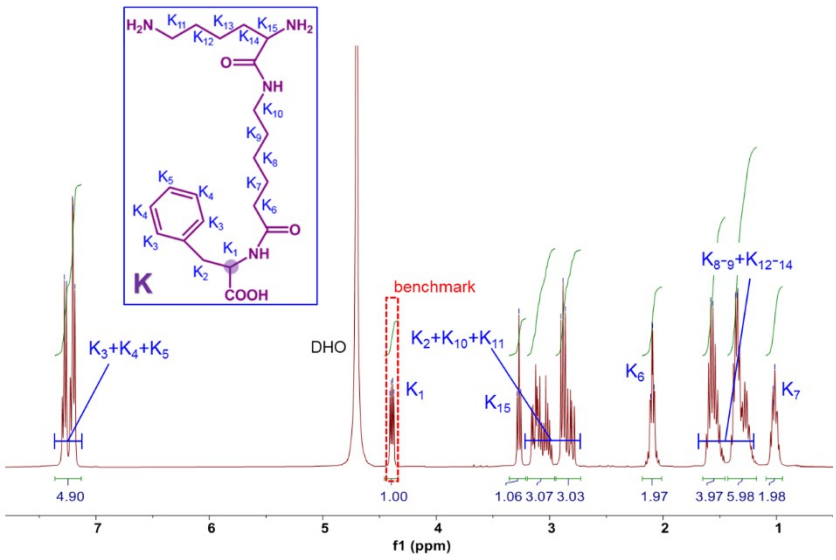

Figure S11. ^{1}H NMR spectrum (D_2O, 600 MHz, δ 7.80~0.50 ppm) of tripeptide with active carboxyl group (K).

PCL with mono hydroxyl functional group (A')[4]

The required PCL was synthesized by anionic ring-opening polymerization of ε-caprolactone (ε-CL), which was shown in Scheme S10. The pre-purified ε-CL by distillation and tert-butyl 3-phenyl-L-alaninate (Phe-OtBu) with $Sn(Oct)_2$ (3%) were added under vacuum into the dried and sealed single flask. Then the reaction mixture was allowed to stir for 24 h at 110 °C under nitrogen atmosphere. After the reaction was finished, few chloroform was used to dissolve the mixture, and then the solution was added to cold methanol. After kept in 4 °C refrigerator overnight, the product was filtered and dried under vacuum.

^{1}H NMR (600 MHz, $CDCl_3$, ppm): δ = 4.75 (m, 1H, A'), 4.06 (t, 40H, A), 3.64 (t, 2H), 3.08 (m, 2H), 2.32 (t, 42H), 1.65 (m, 84H), 1.38 (m, 50H).

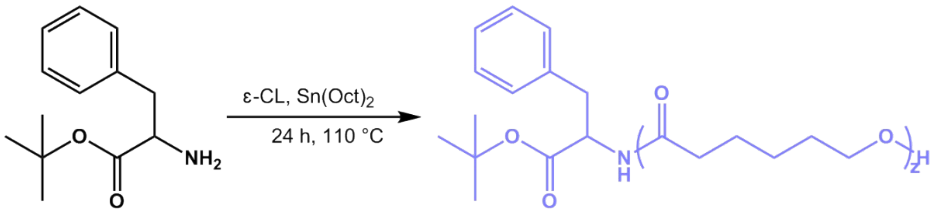

Scheme S10. The synthetic route of PCL with mono hydroxyl group (A').

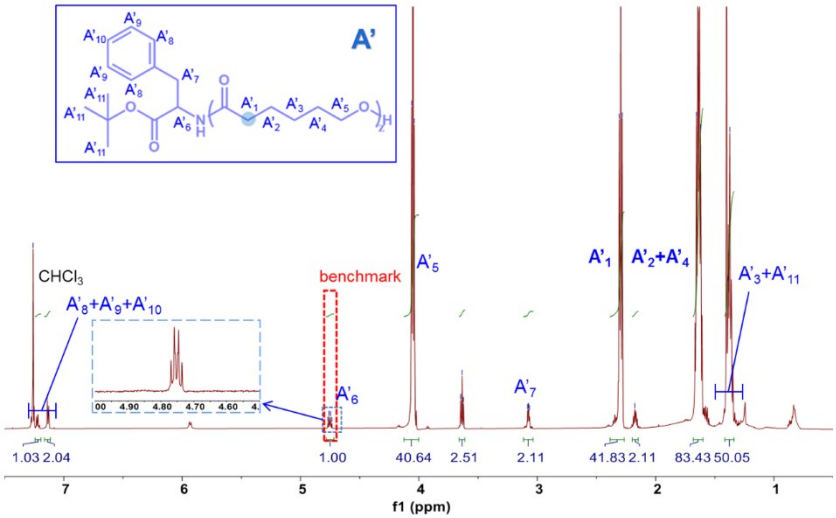

Figure S12. ^{1}H NMR spectrum ($CDCl_3$, 600 MHz, δ 7.50~0.50 ppm) of poly(ε-caprolactone) with active carboxyl group (A').

Note: The peaks at 2.16 ppm is ascribed to the proton of A'$_1$ closest to the initiator, and the signal at 3.07 ppm is assigned to A'$_5$ connected with terminal hydroxyl group.

Calculated M_n of A' based on the integration area of PCL' (-$CH_2C\underline{H}_2$-CO-, 2.32 ppm) with PCL' (-NHC$\underline{H}$CO-, 4.75 ppm) as the benchmark:

M_n (A') = 221 + 114 × I_g/2 ≈ 2,600 g mol^{-1}

2.2.2 Three-segment functional PUs

Compounds 8 (TBK) and 9 (TBQ)

As shown in Scheme S11, the production and purification process was similar to that of **3** (TBABC). Anhydrous DMSO was used to dissolve K and Q segments due to their poor solubility in THF. The target collecting ratios for **8** (TBK) and **9** (TBQ) were 6:1 and 10:3 (chloroform/methanol, v/v), respectively. Yields: ~28% for **8**, and ~22% for **9**.

For **8** (TBK): ^{1}H NMR (600 MHz, $CDCl_3$, ppm): δ = 4.75 (m, 1H, K), 4.20 (m, 4H, B+T), 3.64 (t, 174H, T), 3.38 (s, 3H, T), 3.30-2.90 (s, 10H, B+K).

For **9** (TBQ): ^{1}H NMR (600 MHz, $CDCl_3$, ppm): δ = 4.20 (m, 4H, B+T), 3.64 (t, 164H, T), 3.38 (s, 3H, T), 3.30-2.90 (m, 17H, B+Q), 3.22 (s, 5H, Q), 0.88 (t, 3H, Q).

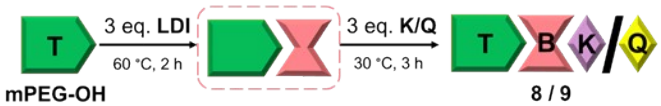

Scheme S11. The synthetic flow diagram of **8** (TBK) and **9** (TBQ) via the diisocyanate chemistry.

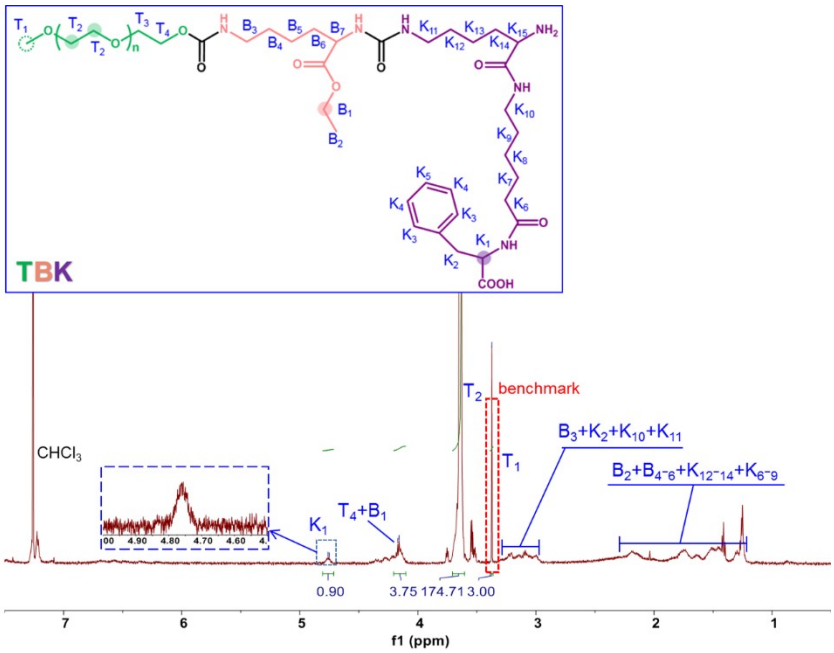

Figure S13. ^{1}H NMR spectrum ($CDCl_3$, 600 MHz, δ 7.50~0.50 ppm) of compound **8** (TBK).

Note: Calculated M_n of compound **8** based on the composition of target chain and the molecular weights of all segments:

M_n (**8**, TBK) = M_n (T) + [M] (B) + [M] (K) = 32 + 44 × I_b/4 + 226 + 406 ≈ 2,500 g mol^{-1}

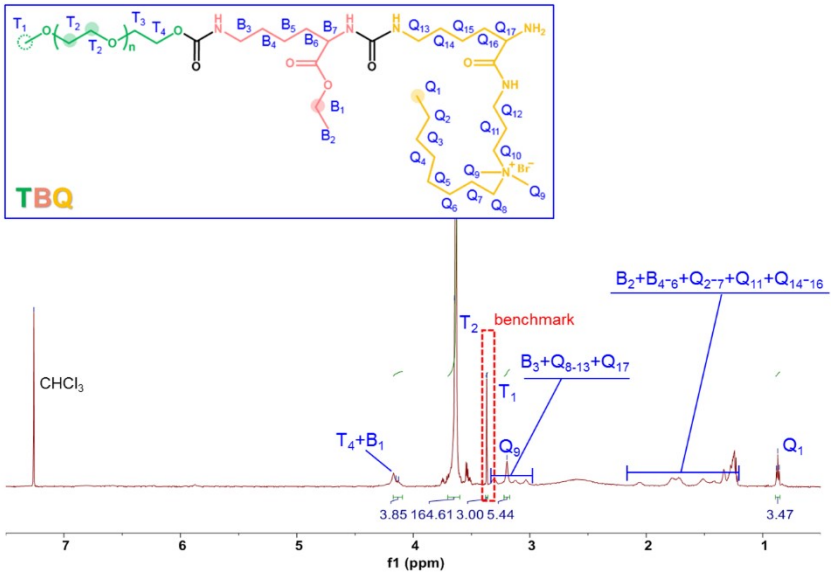

Figure S14. ^{1}H NMR spectrum ($CDCl_3$, 600 MHz, δ 7.50~0.50 ppm) of compound **9** (TBQ).

Note: Calculated M_n of compound **9** based on the composition of target chain and the molecular weights of all segments:

M_n (**9**, TBQ) = M_n (T) + [M] (B) + [M] (Q) = 32 + 44 × I_b/4 + 226 + 423 ≈ 2,500 g mol^{-1}

Compounds 10 (A'BQ) and 11 (A'BK)

As shown in Scheme S12, the production and purification process with A' as the soluble support was

similar to that of **8**. While THF/diethyl ether (1:9, v/v) was used for the refrigeration of the intermediate product (A'B) at -24 °C for 3 h. The target collecting ratios for **10** (A'BQ) and **11** (A'BK) were 10:1 and 15:1 (chloroform/methanol, v/v), respectively. Yields: ~20% for **10**, and ~25% for **11**.

For **10** (A'BQ): ^{1}H NMR (600 MHz, $CDCl_3$, ppm): δ = 4.75 (m, 1H, A'), 4.20 (m, 2H, B), 4.06 (t, 44H, A'), 3.22 (s, 6H, Q), 2.32 (t, 45H, A'), 1.65 (m, 94H, A'), 1.38 (m, 54H, A'), 0.88 (t, 3H, Q).

For **11** (A'BK): ^{1}H NMR (600 MHz, $CDCl_3$, ppm): δ = 4.75 (m, 2H, K+A'), 4.20 (m, 3H, B), 4.06 (t, 45H, A'), 3.22 (s, 6H, Q), 2.32 (t, 45H, A'), 1.65 (m, 96H, A'), 1.38 (m, 55H, A').

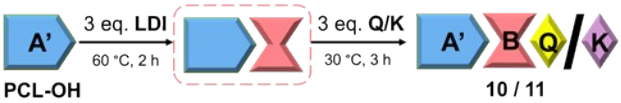

Scheme S12. The synthetic flow diagram of **10** (A'BQ) and **11** (A'BK) via the diisocyanate chemistry.

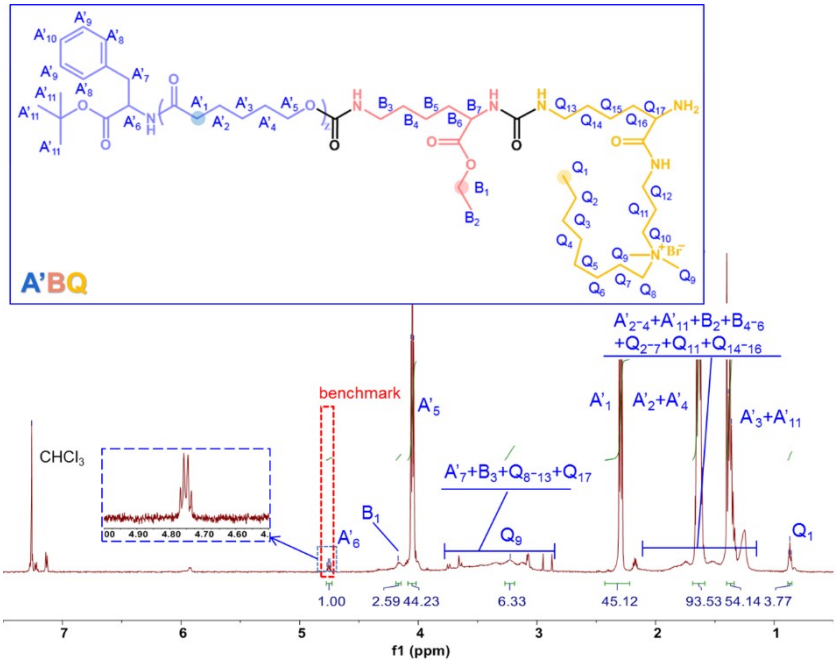

Figure S15. ^{1}H NMR spectrum ($CDCl_3$, 600 MHz, δ 7.50~0.50 ppm) of compound **10** (A'BQ).

Note: Calculated M_n of compound **10** based on the composition of target chain and the molecular weights of all segments:

M_n (**10**, A'BQ) = M_n (A') + [M] (B) + [M] (Q) = 221 + 114 × I_g/2 + 226 + 423 ≈ 3,400 g mol^{-1}

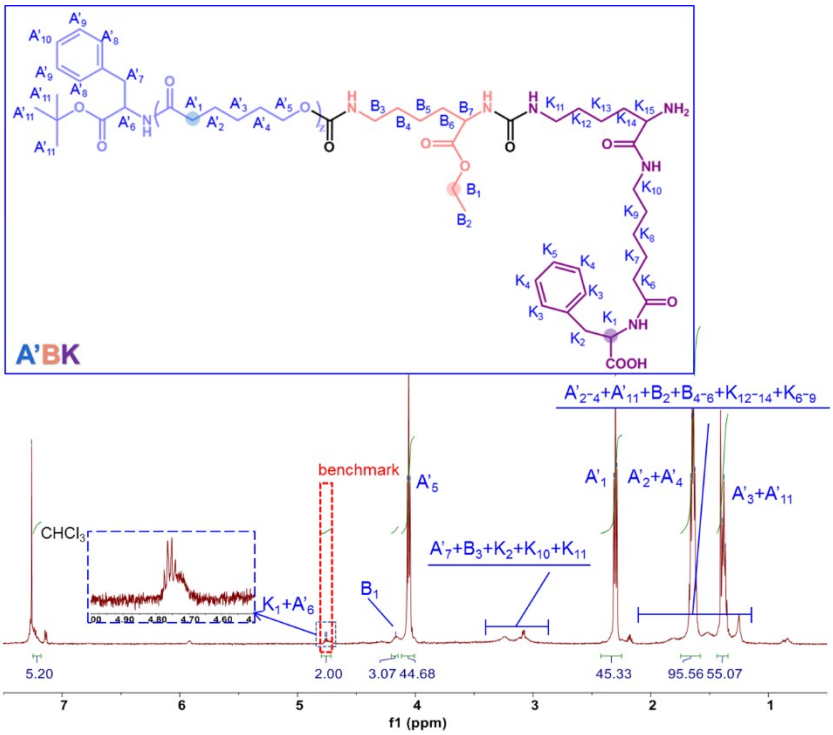

Figure S16. ^{1}H NMR spectrum ($CDCl_3$, 600 MHz, δ 7.50~0.50 ppm) of compound **11** (A'BK).

Note: Calculated M_n of compound **11** based on the composition of target chain and the molecular weights of all segments:

M_n (**11**, A'BK) = M_n (A') + [M] (B) + [M] (K) = 221 + 114 × I_g/2 + 226 + 406 ≈ 3,400 g mol^{-1}

2.2.3 Seven-segment multifunctional PUs with different sequence order

Compound 12 (TBKBQBA', KQ)

Detail descriptions of the synthetic process were provided in the manuscript (experimental methods).

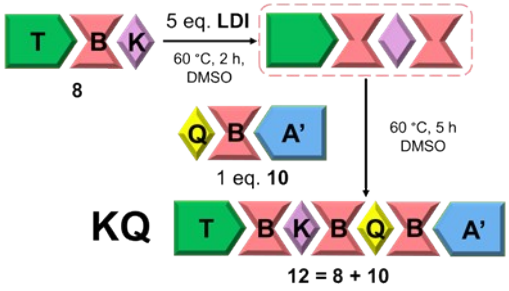

Scheme S13. The synthetic flow diagrams of **12** (KQ) via the convergent strategy: ordered incorporation of model cation segment (Q) and model anion segment (K) into PUs via the established precise synthetic platform.

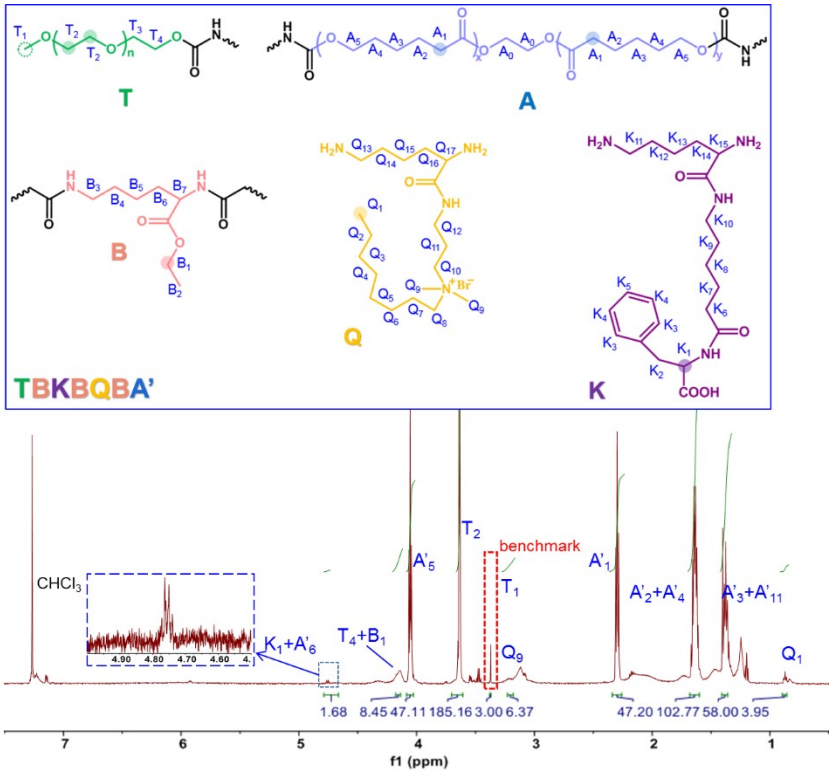

Figure S17. ^{1}H NMR spectrum ($CDCl_3$, 600 MHz, δ 7.50~0.50 ppm) of compound **12** (TBKBQBA', KQ).

Note: Calculated M_n of compound 1**2** based on the composition of target chain and the molecular weights of all segments:

M_n (**12**, TBKBQBA') = M_n (T) + 3 × [M] (B) + [M] (K) + [M] (Q) + M_n (A') = 32 + 44 × I_b/4 + 3 × 226 + 406 + 423 + 114 × I_g/2 + 221 ≈ 6,500 g mol^{-1}

Compound 13 (TBQBKBA', QK)

As shown in Scheme S14, the synthetic process of **13** was similar to that of **12**. Briefly, the reaction of dried **9** (TBQ, 1 mmol) and LDI (B, 5 mmol) with organic bismuth dissolved in anhydrous DMSO were performed at 60 °C for 2 h under nitrogen environment. After the reaction was finished, the reaction solution was added into anhydrous diethyl ether with stirring, and the solution was refrigerated at -24 °C for 2 h. The intermediate product (TBQB) was quickly collected by suction filtration and washed twice with diethyl ether. Then dried TBQB and **11** (A'BK, 1 mmol) with organic bismuth dissolved in DMSO was reacted at 60 °C for 5 h under nitrogen environment. Finally, the similar purification procedure was conducted for compound **13** (TBQBKBA', QK), and the target collecting ratio was about 7:1 (v/v) to give white solid (~23% yield).

^{1}H NMR (600 MHz, $CDCl_3$, ppm): δ = 4.75 (m, 2H, K+A'), 4.20 (m, 8H, B+T), 4.06 (t, 49H, A'), 3.64 (t, 163H, T), 3.38 (s, 3H, T), 3.22 (m, 6H, Q), 2.32 (t, 50H, A'), 1.65 (m, 104H, A'), 1.38 (m, 62H, A'), 0.88 (t, 3H, Q). ^{13}C NMR (600 MHz, $CDCl_3$, ppm): δ = 173.5, 173.2, 172.4, 171.3, 158.1, 137.9, 129.6, 128.5, 126.8, 80.9, 71.8, 70.3, 63.9, 60.7, 58.5, 54.4, 52.9, 50.5, 40.0, 37.4, 35.3, 33.8, 32.1, 31.6, 30.1, 29.0, 28.3, 28.0, 25.4, 24.6, 22.9, 22.5, 14.5.

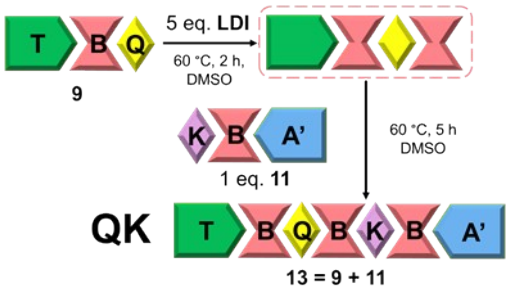

Scheme S14. The synthetic flow diagrams of **13** (QK) via the convergent strategy: ordered incorporation of model cation segment (Q) and model anion segment (K) into PUs via the established precise synthetic platform.

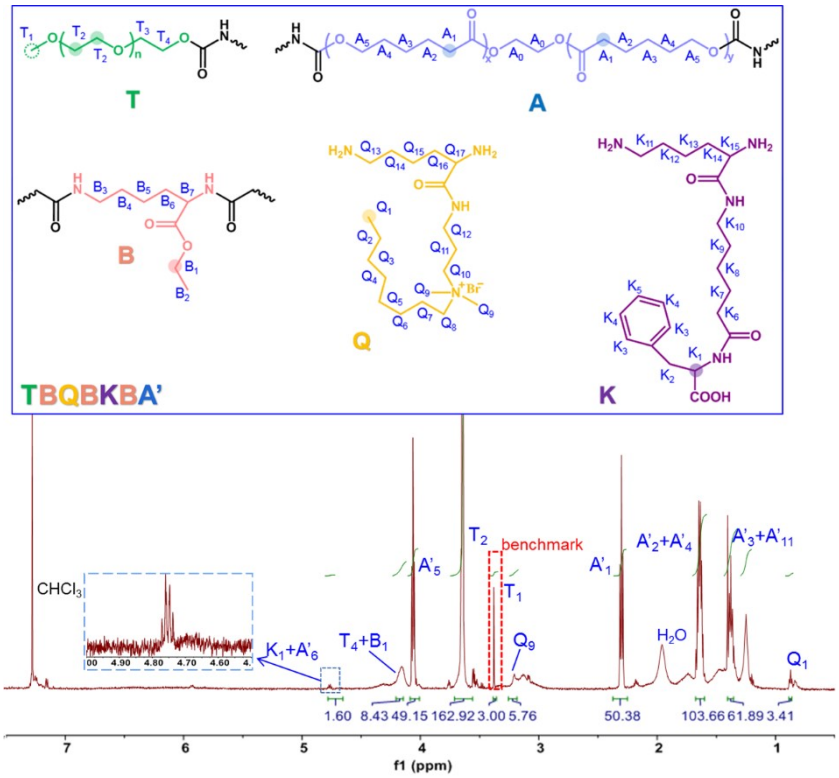

Figure S18. ^{1}H NMR spectrum ($CDCl_3$, 600 MHz, δ 7.50~0.50 ppm) of compound **13** (TBQBKBA', QK).

Note: Calculated M_n of compound **13** based on the composition of target chain and the molecular weights of all segments:

M_n (**13**, TBQBKBA') = M_n (T) + 3 × [M] (B) + [M] (K) + [M] (Q) + M_n (A') = 32 + 44 × I_b/4 + 3 × 226 + 406 + 423 + 114 × I_g/2 + 221 ≈ 6,400 g mol^{-1}

Section 2.3 Experimental Protocols

2.3.1 Self-Assembly of PUs

Self-assembly of PU structure was performed by a dialysis method. Briefly, 1 mL of PU solution dissolved in DMAc (10 mg mL^{-1}) was added dropwise into 4 mL of distilled water under ultrasonic (60% power). Then the organic solvent was removed by dialysis (MWCO 3500) against distilled water for 72 h, changing the external water once 3 h. Finally, the resulting solution was centrifugalized for 10 min at 3000 r min^{-1} and the supernatant was filtered through a 0.45 μm pore-sized syringe filter (Jinteng, China).

2.3.2 Pyrene Fluorescence Probe Study

The critical aggregation concentration (CAC) values of polymer assemblies were measured by a fluorescence method using pyrene as a probe. Briefly, 200 μL of acetone solutions of pyrene (5.0×10^{-6} mol L^{-1}) were transferred into the vials and acetone was evaporated under argon flow. Then 2 mL of polymer self-assemblies with different concentrations were added into the vials and the mixture was sonicated at room temperature for 3 h. The steady-state fluorescence excitation spectra (λ_{ex}) from 300 to 360 nm with the emission wavelength (λ_{em}) at 372 nm were recorded on a FluoroMax-4 spectrophotometer (HORIBA, Ltd., Japan), and the bandwidths for excitation and emission spectra were both 5 nm.

2.3.3 Protein Adsorption Experiment

The samples were prepared by mixing naked micelles (500 μg mL^{-1}) with various accurate concentrations of bovine serum albumin (BSA) solution in ultrapure water. After they were incubated in an incubator shaker at 25 °C for 24 h, the changes of zeta potentials were conducted directly. To quantify the amount of protein absorption by the enhanced BCA protein assay kit, the non-adsorbed BSA in the supernatant was separated by centrifugation (12 000 krcf, 10 min).

2.3.4 DOX Loading and Release

Fluorescent DOX was used as the model hydrophobic anticancer drug. In brief, PUs and DOX·HCl desalted by excess amount of TEA with 20% feed ratio were dissolved in DMAc under ultrasonic condition. The subsequent process was the same as the self-assembly of PUs. The amount of DOX loaded was determined by the absorption at 488 nm on an UV-3600 spectrophotometer (Shimadzu Corporation).

Drug loading content and encapsulation efficiency were calculated according to the following equations:

Loading content (LC, %) = weight of loaded drugs / weight of drug-loaded micelles × 100%

Encapsulation efficiency (EE, %) = weight of loaded drugs / weight of feeding drugs × 100%

The release profiles of DOX from PU micelles were evaluated with a dialysis method. Briefly, the dialysis bag containing drug-loaded micelles was immersed in phosphate buffer solution (PBS, 0.01 M, pH 7.4) at 37 °C in an incubator shaker. At desired time intervals, 6 mL of release media was sampled and replenished with an equal volume of fresh buffer solution. The amount of DOX released was quantified by the FluoroMax-4 spectrophotometer above mentioned. The release experiments were conducted in triplicate.

2.3.5 Cell Internalization

The cellular uptake of DOX-loaded PU micelle was conducted by flow cytometry (FCM) and a confocal laser scanning microscope (CLSM), and cervical cancer (HeLa) cell line was selected for the tests. For CLSM, HeLa cells were seeded in the confocal small dishes at a density of 3×10^4 cells per dish and cultured in DMEM media (supplemented with 10% fetal bovine serum, 1% penicillin-streptomycin solution and C0290M mycoplasma removal agent) overnight. Then the DOX-encapsulated micellar solutions were added separately into the dished with a consistent drug concentration of 10 μg mL^{-1} and incubated with the cells for the set time (1h,3 h and 6 h). Next, after the medium removed, the cells were washed with cold PBS for three times, fixed with 4% formaldehyde at 4 °C for 15 min and stained with DAPI (10 μg mL^{-1}) at room temperature for 5 min. Finally, the cells were covered with PBS and observed by a Zeiss 880 LSM Microscope (Carl Zeiss AG, German). For FCM, HeLa cells were seeded in a six-well plate with 10×10^5 cells per well and cultured with DMEM media overnight. Then DOX-labeled micellar solutions with the consistent drug concentration of 10 μg mL^{-1} were added and incubated with the cells for the corresponding time. After removing the medium, the cells

were washed with PBS for three times, digested by trypsin, centrifuged, and re-suspended in 0.5 mL PBS for flow cytometer measurement (BD LSRFortessa, USA).

2.3.6 MTT Assay

MTT assay was performed to evaluate the cytotoxicity of the naked micelles and the therapeutic efficacy of DOX-loaded formulations against HeLa and normal cells (fibroblast L929). Briefly, HeLa cells were seeded into 96-well plates with a density of 2×10^3 cells per well and cultured with DMEM media for 12 h. Then, the cells were incubated with the naked micellar medium solution at different concentrations and the DOX-encapsulated micellar medium solution containing various DOX concentrations for 3 d, respectively. At the determined time, 20 μL of MTT solution (5 mg mL^{-1}) was added into each well for another 4 h of incubation. Finally, the culture solution in each well was replaced by 200 μL of DMSO, which was used dissolve the formed formazan crystals after shaking the plates for 10 min, and the absorption intensity at 492 nm was recorded on a Synergy™ LX Multi-Mode Microplate Reader (BioTek, USA). Untreated cells in culture media were set as negative control with 100% viability. All the measurements were performed in triplicate.

2.3.7 Animals

Male nude mice (15 ± 1 g) were obtained from the Laboratory Animal Center of Sichuan University (Sichuan, China). They were free to access standard food and water in a light-controlled room at 25 ± 2 °C with the humidity of 55 ± 5%. The animal protocols were approved by the Ethics Committee of Sichuan University and in accordance with the Principles of Laboratory Animal Care of the National Institutes of Health, China.

Mouse tumor models: Each mouse was injected subcutaneously with 2×10^6 HeLa cells in 0.1 mL pure DMEM medium at the upper flank of right hind leg. Nude mice were randomly grouped (n = 5) according to tumor volume when the tumors had grown to 30-50 mm3. Tumor volume was calculated using the equation V = ab2/2, where “a” and “b” represent the length and the width of the tumors, respectively.

2.3.8 Tissue Distribution

To assess the tissue distribution of different micelles in vivo, HeLa tumor-bearing mice were injected with DOX-labeled micellar solution at a DOX dose of 1 mg kg^{-1} in caudal vein. Then the heart, liver, spleen, lung, kidney and tumor were collected from killed mice after treatment for 3 h. In the end, the semiquantitative analysis of the fluorescence intensity at the tumor site was also detected by in vivo image system (IVIS Lumina III, PerkinElmer, USA).

2.3.9 Antitumor Activity in Vivo

The nude mice bearing HeLa tumors were randomly assigned to five groups (n = 5), and intravenously injected via tail vein with 150 μL of DOX-loaded micellar formulations every 3 d at a DOX dose of 2 mg kg^{-1}. To achieve this dosage, the DOX-loaded micelles with high PU concentration (4 mg mL^{-1}) was prepared by feeding 20% of DOX, followed by dialysis against PBS (pH 7.4, 10 mM) for 72 h. The final amount of DOX was determined by UV spectrophotometer (Section S2.3.4) and adjusted with PBS to the required concentration. For comparison, mice injected with PBS, drug-free assemblies and free DOX were set as negative, blank and positive controls, respectively. Meanwhile, tumor size, tumor volume, survival rate and body weight were also recorded every 3 d. On the day of 15, all the mice were sacrificed by cervical dislocation under deep anesthesia and the tumors were excised and weighted. Besides, the tumor tissues after treatment were stained with hematoxylin and eosin (H&E) for histological examination. The tumor weight inhibition rate (TWI) was calculated using the following equation:

TWI = (the average tumor weight of negative control group – the average tumor weight of experiment group) / the average tumor weight of negative control group × 100%.

2.3.10 Statistical Analysis

The quantitative data obtained were expressed as means ± standard deviations (SD). The significance of difference was analyzed by one or two-way analysis of variance (ANOVA) using the Statistical Package for the Social Sciences (SPSS, version 19) software. Statistically significant difference was evaluated with $*P < 0.05$, and there was no significant difference if P-value was greater than 0.05.

Section 3. Supplementary Figures

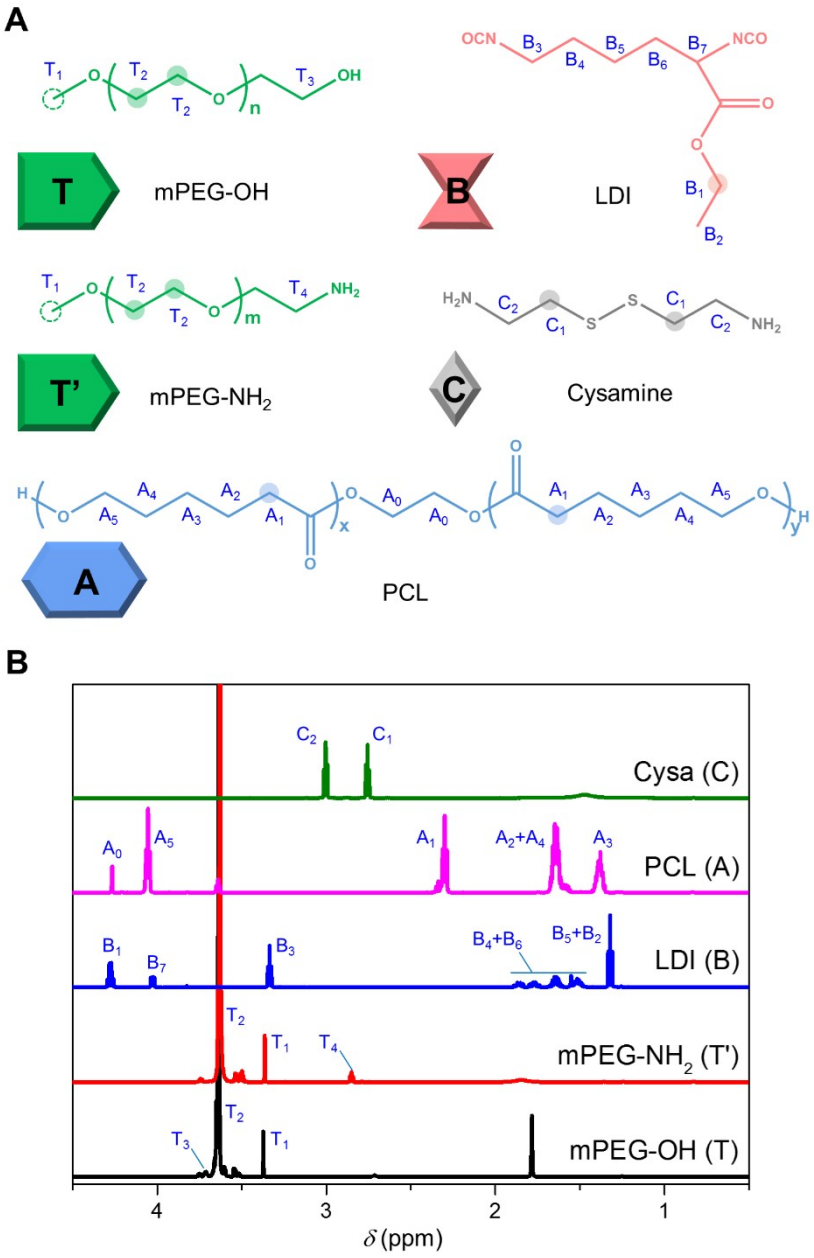

Figure S19. (A) Repensentative difunctional modules without protection. (B) Stacked ^{1}H NMR spectra ($CDCl_3$, 600 MHz, δ 5.00~0.50 ppm) of typical model PU segments.

Note: The characteristic chemical shifts of various segments are T/T' (T_1, C$\underline{H}_3$-O-, 3.38 ppm; T_2, -O-C$\underline{H}_2$C$\underline{H}_2$-O-, 3.64 ppm), B (B_1, $CH_3C\underline{H}_2$-O-, 4.20 ppm; B_2, C$\underline{H}_3CH_2$-O-, 1.26 ppm), A (A_5, -O-C$\underline{H}_2$C$\underline{H}_2$-O-, 4.27 ppm; A_0, -O-C$\underline{H}_2CH_2CH_2$-, 4.06 ppm; A_1, -$CH_2C\underline{H}_2$CO-, 2.32 ppm; A_2+A_4, -O-$CH_2C\underline{H}_2CH_2C\underline{H}_2CH_2$-CO-, 1.64 ppm; A_3 -O-$CH_2CH_2C\underline{H}_2CH_2CH_2$-CO-, 1.38 ppm) and C ($C_1$, -$CH_2C\underline{H}_2$-S-S-C$\underline{H}_2CH_2$-, 2.82 ppm), and they are used to determine the compositions and calculate the molecular weights of synthetic products.

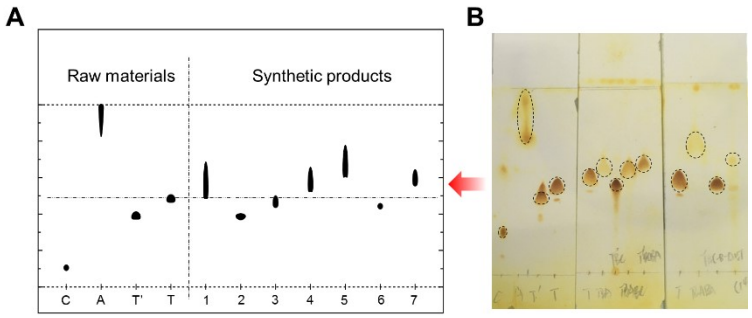

Figure S20. (A) TLC diagram and (B) original image of different compounds colored by iodine.

Note: The volume ratio of the eluting agent is chloroform: ethyl acetate: methanol: ammonia = 40: 8: 8: 1. The TLC is used not only to monitor the purification of crude products, but also to estimate the reaction endpoint for higher productivity. Before carrying out TLC in the later stage of the reactions, ethylenediamine and ethanolamine are respectively used to neutralize the unreacted isocyanate (NCO) of mono-hydroxy and mono-amino derived intermediates, which are purified simply by diethyl ether precipitation.

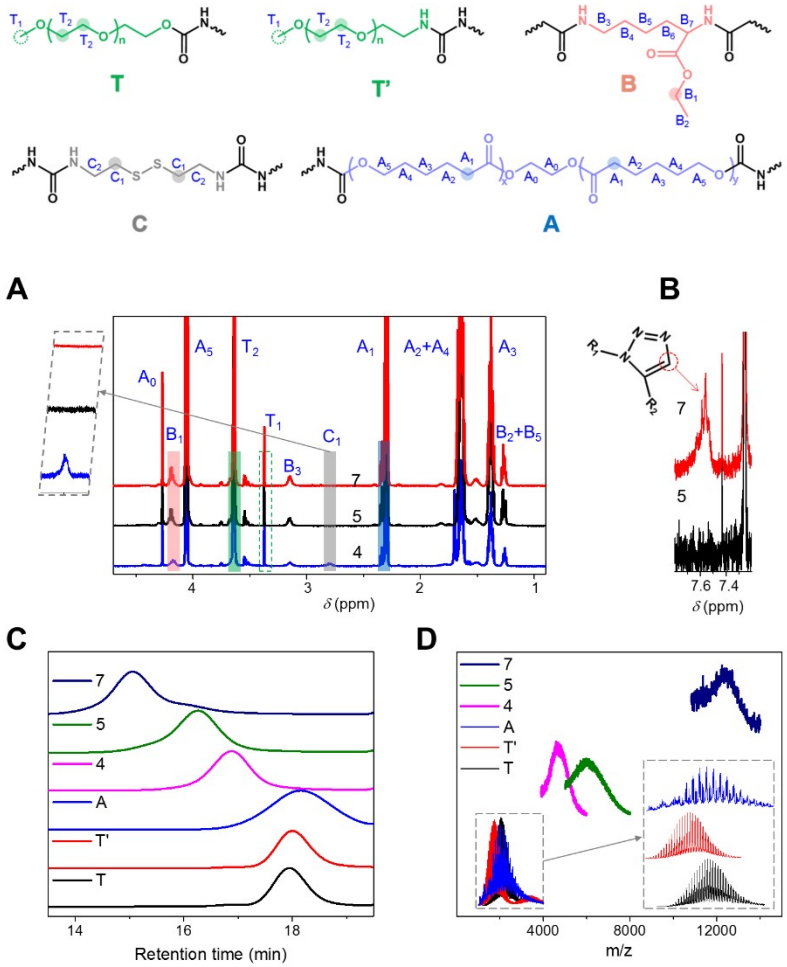

Figure S21. (A) Stacked ^{1}H NMR spectra ($CDCl_3$, 600 MHz, δ 4.70~0.90 ppm) of different synthetic compounds with the characteristic protons highlighted. (B) Characteristic proton peak ($CDCl_3$, 600 MHz, δ 7.80~7.20 ppm) of triazole in **7** compared with **5**. (C and D) GPC traces (C) and MALDI-TOF MS spectra (D) of different synthetic compounds. Insert (D): enlarged TOF MS spectra of raw materials.

Note: For NMR, the appearances of characteristic signals confirm the successful incorporation of target model segments (Figure S21A), and the data of calculated M_n by the integration areas further verifies the well-defined structures of products (Table S1). The peak at 7.56 ppm (Figure S21B), belonging to the characteristic proton signal of triazole (NR_1-N=N-$C\underline{H}$=CR_2) in compound **7** (TBABABC'-C''BABABT), indicates the success of azido-alkyne click chemistry, demonstrating the huge potential of preparing the precise PU with high molecular weight by efficient convergent approaches. From the measurements (Figures S21C and S21D), the molecular weights of PUs increase regularly as expected with the iterative diisocyanate reactions and click chemistry going on.

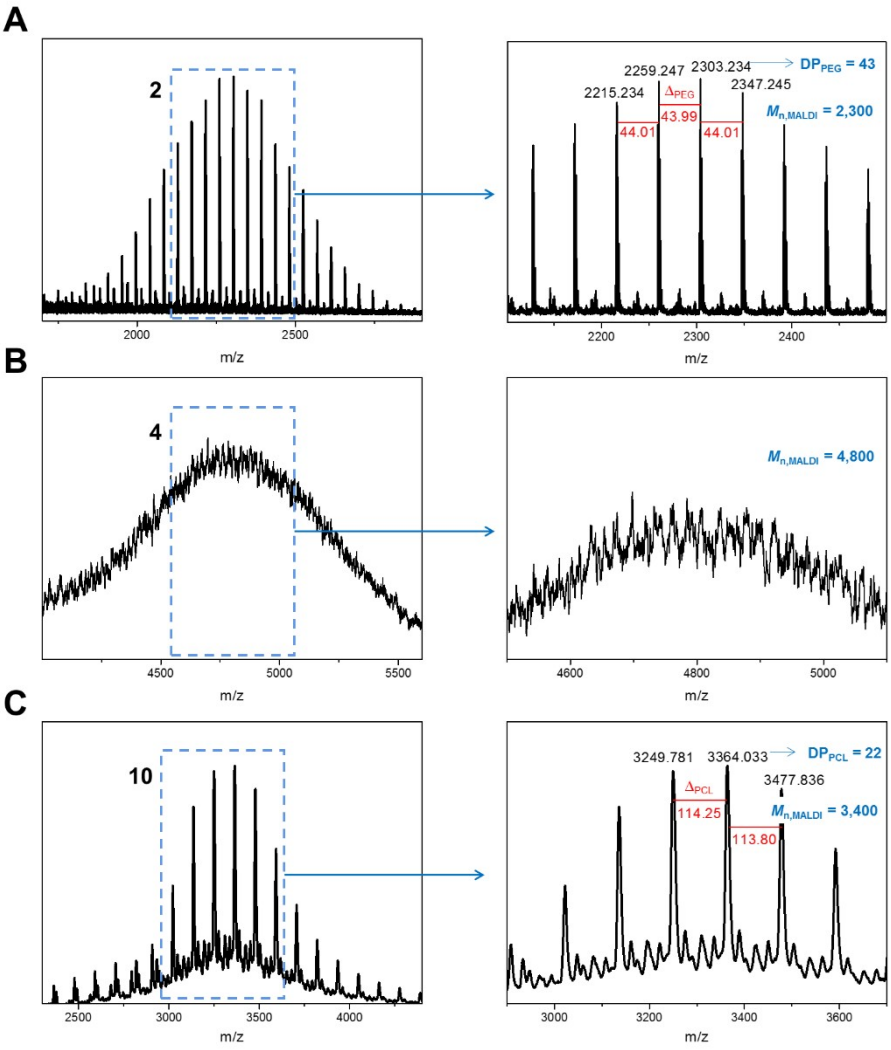

Figure S22. Analysis of enlarged representative MALDI-TOF spectra for compound **2** (A), compound **4** (B) and compound **10** (C). Right spectra are enlarged details for the dotted ranges.

Note: The characteristics of repeat units for compound **2** (-CH_2CH_2O-, an interval of 44) and **10** (-$OCH_2CH_2CH_2CH_2CO$-, an interval of 114) are apparent, since there is only one segment with repeat unit in the structures and the others are small molecules with accurate molecular weight. Moreover, the observed peaks of m/z are in good agree with the theoretical calculation by rational degree of polymerization (DP). Once two segments with different repeat units are in a single chain, the features are plunged into chaos and difficult to distinguish. The number-average molecular weights are estimated form the dominant peaks.

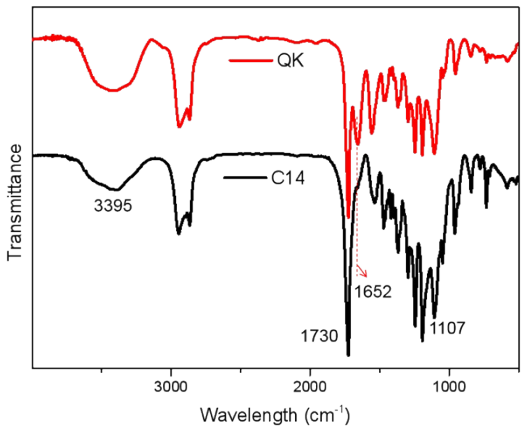

Figure S23. FT-IR spectra of representative compounds **7** and **13**.

Note: Broad stretching bands observed at 3200-3600 cm^{-1} and 2800-3000 cm^{-1} are attributed to N-H and C-H stretching vibration, respectively. The peak at 1107 cm^{-1} can be associated to the C-O-C stretching vibrations of PEG. The stretching band in the 1600-1800 cm^{-1} (1730 cm^{-1}) region is due to the absorption of ester carbonyl groups of PCL and free and hydrogen-bonded carbonyl of urethane groups, where a shoulder observed at 1652 cm^{-1} is ascribed to the hydrogen-bonded carbonyl of urea groups. The characteristic signals are distinctly appeared in the spectra of compounds **7** and **13** except for the peak at 1652 cm^{-1} for compound **7**, which contains no diamine segments (Q and K) to form urea groups.

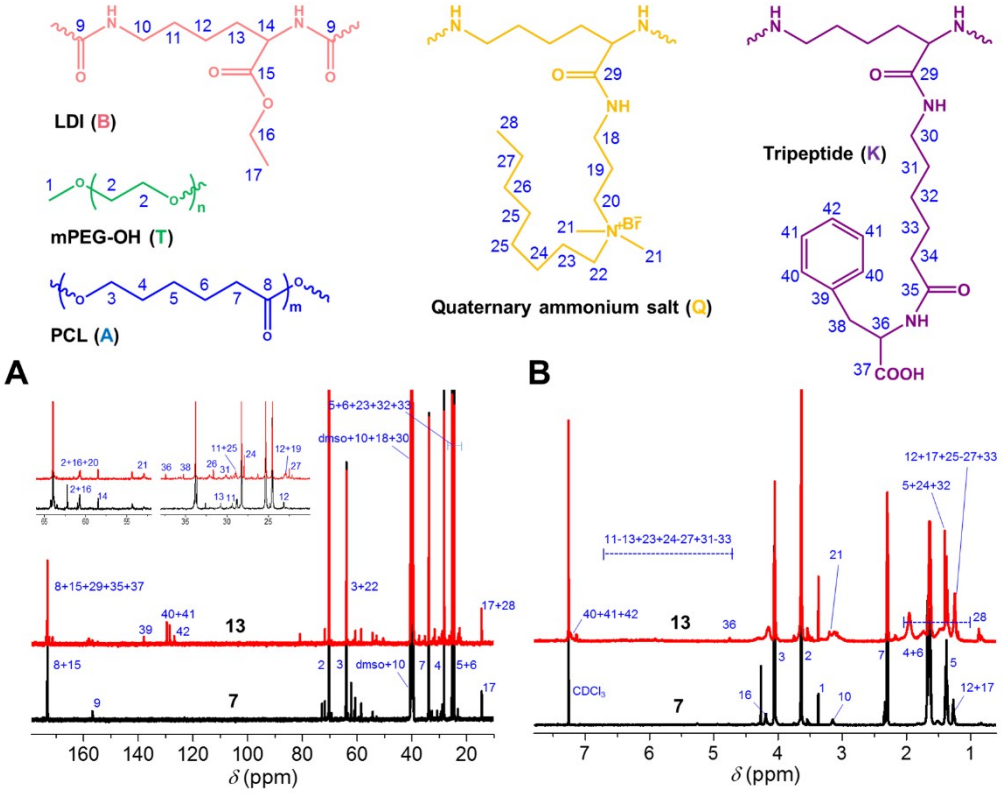

Figure S24. ^{13}C NMR spectra (DMSO-d_6, 600 MHz, δ 179.0~10.0 ppm) (A) and ^{1}H NMR spectra ($CDCl_3$, 600 MHz, δ 7.80~0.60 ppm) of compound **7** (black line) and **13** (red line). Insets show the partially enlarged spectra.

Note: In ^{13}C NMR spectra, the ^{13}C resonance signals at 173.1, 64.0, 33.8, 28.3, 25.4 and 24.6 ppm are assigned to the six carbons of PCL unit. The peak at 70.3 ppm is ascribed to PEG segment. The signals at 156.8 and 14.1 originate from LDI monomer. The peaks at 137.9, 129.6, 128.5, 126.8, 37.4, 35.2 and 30.1 ppm derived from anion segment (K) and at 52.9, 50.5, 31.7, 28.0, 22.5 ppm assigned to cationic segment (Q) in the spectrum of compound **13** cannot be found in that of compound **7**. For ^{1}H NMR spectra, detail analyses have been provided in the experimental section. The peaks appeared in the ranges of 2.00~1.00 ppm are difficult to identify and analysis because of the serious overlay and interference by each other.[5]

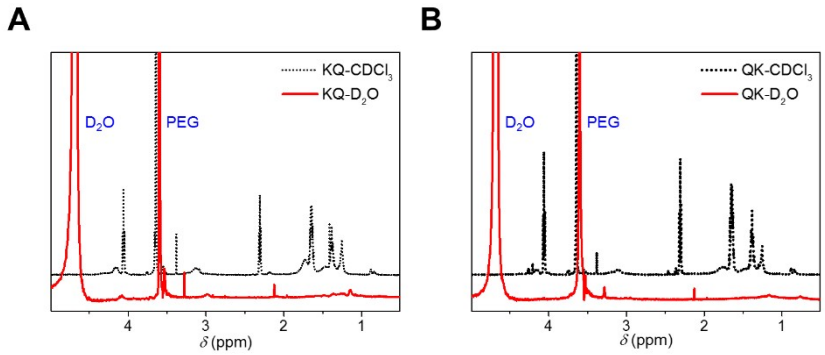

Figure S25. ^{1}H NMR (600 MHz, δ 5.00~0.50 ppm) of lyophilized KQ (A) and QK (B) self-assembly redissolved in D_2O after compared to original spectra in $CDCl_3$.

Note: Compared to the diverse signals in $CDCl_3$, these spectra of KQ and QK in D_2O exhibit apparent peaks of PEG and significantly weakened resonances of PCL, which suggests that core-shell micellar structures with an isolated hydrophobic PCL inner core and a hydrophilic PEG outer shell.[2]

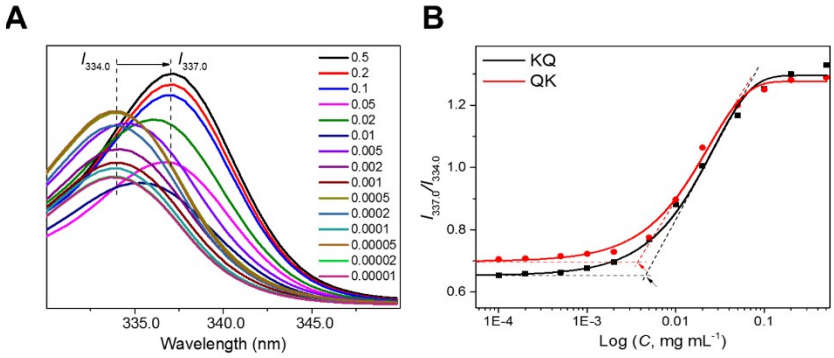

Figure S26. (A) Pyrene excitation spectra (λ_{em} = 373.0 nm) at various concentrations of QK nanoparticles. (B) Ratios of $I_{337.0}$ / $I_{334.0}$ from pyrene excitation spectra as a function of the concentrations (log *C*) in aqueous solution. The CAC values are obtained from the intersection of the two trend lines shown by the arrows.

Note: The (0,0) absorption band in the excitation spectra shifts from 334.0 to 337.0 nm with the increase of polyurethane concentration in an aqueous solution of pyrene (Fig. S26A), suggesting that pyrene molecules are transferred from water environment to hydrophobic core of the nanoparticles. The sequence-defined multifunctional PU chains (KQ and QK) are equipped with the similar ability to form micelles, as their CACs are very close (Fig. S26B, Table S6).

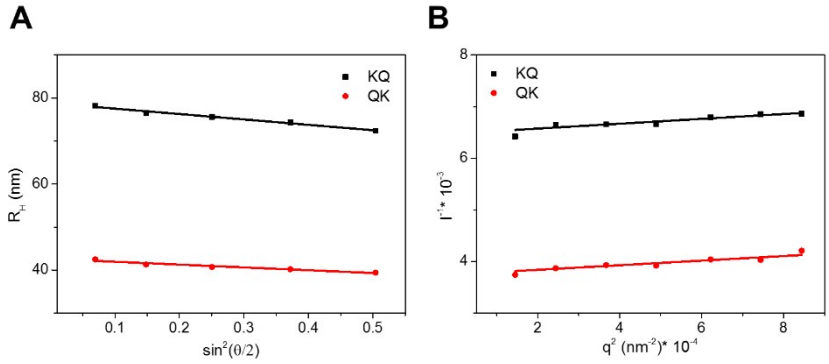

Figure S27. (A) Hydrodynamic radius associated functions at different incident angles determined by DLS. (B) Typical Berry plots of KQ and QK assemblies measured at 25 °C using multi-angle SLS.

Note: As shown in Table S6, the hydrodynamic radius (R_H) values of KQ and QK assemblies are determined to be 73.8 and 53.1 nm, respectively. Besides, the radius of gyration (R_G) values of KQ and QK assemblies are measured to be 51.2 and 39.9 nm, respectively. Therefore, the characteristic parameters ($\rho = R_G/R_H$), which is sensitive to the particle morphology, of KQ and QK assemblies are found to be 0.72 and 0.78 nm, respectively. They are close to 0.775 and indicative of spherical micellar morphologies rather than vesicular structures ($\rho \approx 1.0$). [6,7]

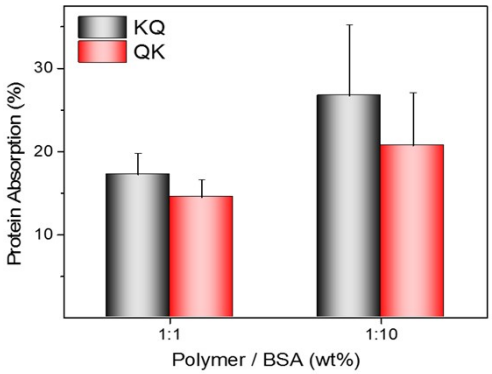

Figure S28. BSA absorption amount of sequence-defined multifunctional PU micelles incubated with different ratios of polymer/BSA (wt%).

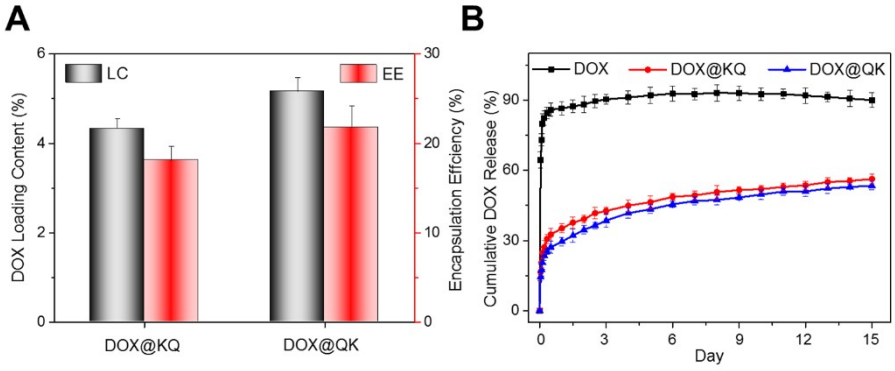

Figure S29. (A) Drug loading capacity of different PU micelles with 20% drug feed ratio. (B) Drug release

profiles of different DOX-loaded micelles in PBS buffer (0.01M, pH 7.4).

Note: As shown in the Fig. S29A, QK micelles exhibit higher DOX-loading capacity compared to KQ micelles. Moreover, DOX@QK and DOX@KQ exhibited similar release profiles, with more than 70% of drugs released within 15 d (Fig. S29B).

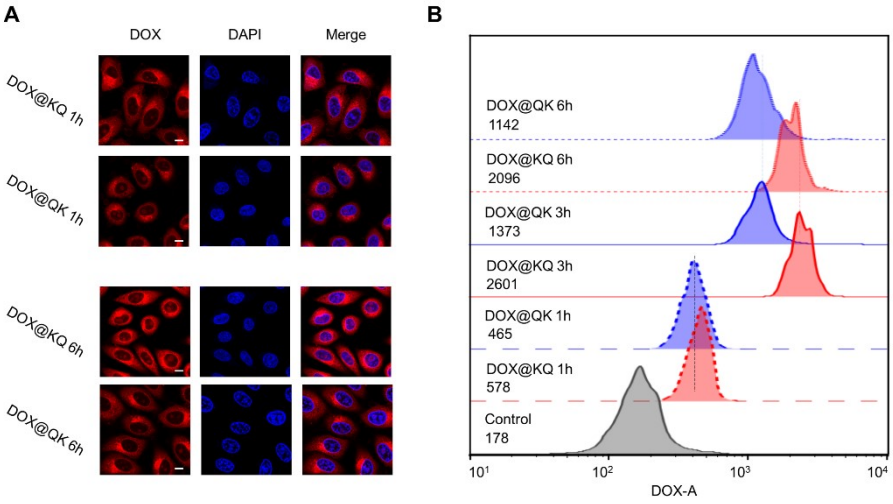

Figure S30. (A) Confocal images of HeLa cells incubated with DOX-loaded micelles for 1 h and 6 h. The scale bars are 10 μm. (B) FCM histograms of HeLa cells incubated with DOX-labelled micelles at the DOX concentration of 10 μg mL^{-1} for different times. Untreated cells are used as the control group, and the numerical values are the statistical mean values (∑mean) of DOX-Area.

Note: As shown in Fig. 4A and S30, DOX@KQ displays faster cellular uptake compared to DOX@QK both in 1 h and 3 h, and the difference of fluorescence intensity gradually increases. However, when incubation with 6 h, a certain degree of attenuation is happened to the fluorescence intensities of two samples, which might cause by the dominant exocytosis.

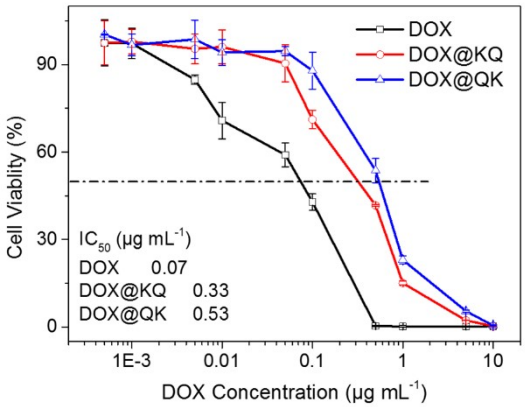

Figure S31. Cell viability of HeLa cells incubated with DOX@KQ and DOX@QK at various DOX concentrations for 72 h in vitro. Free DOX is used as a positive control.

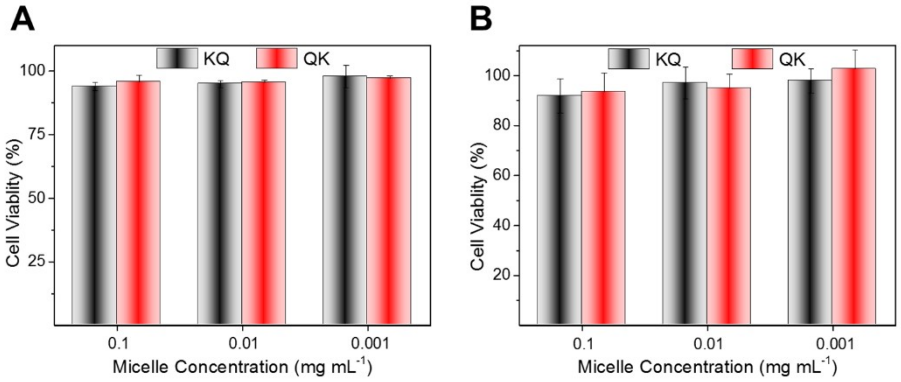

Figure S32. Cytotoxicity of L929 mouse fibroblasts (A) and HeLa cells (B) incubated with drug-free micelles at different concentrations for 72 h.

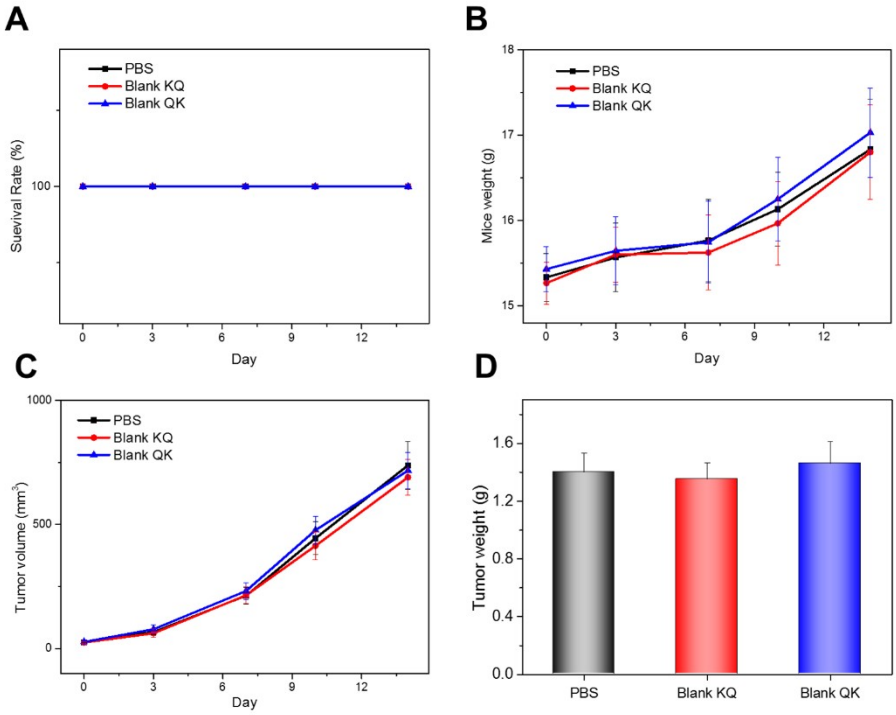

Figure S33. Changes of survival rate (A), mice weight (B) and tumor volumes (C) of nude mice receiving intravenous administration of drug-free blank nanocarriers at the same polymer concentration of drug nanoformulations. (D) Mean weights of tumors separated from mice treated with blank micelles for 2 weeks. Error bars represent SD, n = 5.

Note: It is obvious that blank nanoparticles show no significant effects on mice life and tumor growth in contrast with PBS group.

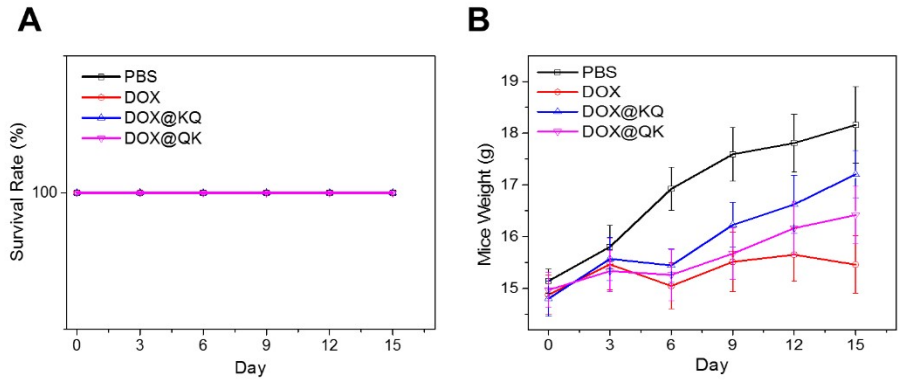

Figure S34. The changes of survival rate (A) and body weight (B) of HeLa tumor-bearing nude mice during the intravenous medication every three days for two weeks at a DOX dose of 2 mg kg^{-1}. The data are presented as the average ± standard error (n = 5).

Note: During the therapeutic period, no mice died (Fig. S34A) and no apparent weight loss (Fig. S34B) was observed probably due to the relative low dose of DOX, suggesting that the administrations of drug therapy have negligible influence on their normal life.

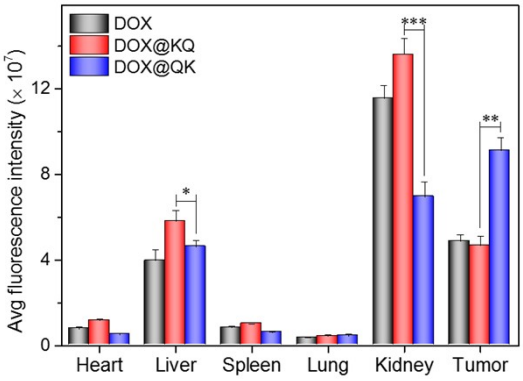

Figure S35. Ex vivo semiquantitative average fluorescence intensities of excised organs of HeLa tumor-bearing nude mice after intravenous injection with DOX-labelled micelles.

Section 4. Supplementary Tables

Table S1. Integration areas of different characteristic chemical shifts (ppm) of model PUs

Samples	Area ratios						Calculated M_n (g mol^{-1})
	4.27	4.20	3.64	3.38	2.82	2.32	
T	-	-	185.00	3.00	-	-	2,100
T’	-	-	156.00	3.00	-	-	1,800
A	4.00	-	-	-	-	39.00	2,200
1	4.00	4.00	191.00	3.00	-	35.00	4,400
2	-	2.00	158.00	3.00	4.00	-	2,200
3	4.00	6.00	174.00	3.00	4.00	43.00	5,000
4	4.00	4.00	163.00	3.00	4.00	42.00	4,900
5	7.00	7.00	179.00	3.00	-	68.00	6,500
6	4.00	7.00	365.00	6.00	4.00	31.00	6,700
7	16.00	16.00	364.00	6.00	-	138.00	13,700

Note: The signals at 4.27 ppm, 3.64 ppm, 3.38 ppm, 2.82 ppm and 2.32 ppm are corresponding to A_0 (A, -O-C$\underline{H_2}$C$\underline{H_2}$-O-), T_2 (T/T’, -O-C$\underline{H_2}$C$\underline{H_2}$-), T_1 (T/T’, C$\underline{H_3}$-O-), C_1 (C, -CH_2C$\underline{H_2}$-S-S-C$\underline{H_2}$$CH_2$-) and A_1 (A, -CH_2CH_2C$\underline{H_2}$-CO-), respectively (Figure S19). The proton of T_1 (T/T’, C$\underline{H_3}$-O-, 3.38 ppm) was used as the quantitative benchmark for other protons, and the integration areas are used to determine the compositions and calculate the number-average molecular weights (M_n) of synthetic products. Besides, the signal of 4.20 ppm originates from both B_1 (B, CH_3C$\underline{H_2}$-O-) and T_3 (T, -CH_2C$\underline{H_2}$-OH), so that the integral area of compound **1** (TBA) (Fig. S1) is about 2 larger than that of compound **2** (T’BC) (Fig. S2). Small amount of numerical deviation, dating from the integration and data processes, are acceptable.

Table S2. Relative molecular weights of model PUs measured by GPC

Samples	M_n (g mol^{-1})	M_w (g mol^{-1})	$Đ$ (= M_w/M_n)
T	5,500	5,800	1.06
T’	5,200	5,500	1.06
A	4,900	5,400	1.11
1	9,700	10,600	1.09
2	6,000	6,500	1.08
3	12,000	12,800	1.07
4	10,700	11,900	1.10
5	16,200	17,500	1.08
6	17,000	18,000	1.06
7	31,400	35,500	1.13

Table S3. Integral areas of different characteristic chemical shifts (ppm) of multifunctional PUs with different sequence orders of functional segments

Samples	Area ratios					Calculated M_n (g mol^{-1})
	4.75	3.64	3.38	2.32	0.88	
A’	1.00	-	-	42.00	-	2,600
8	1.00	178.00	3.00	-	-	2,500
9	-	164.00	3.00		3.00	2,500
10	1.00	-	-	46.00	4.00	3,400
11	2.00	-	-	49.00	-	3,400
12	2.00	182.00	3.00	47.00	4.00	6,500
13	2.00	169.00	3.00	50.00	3.00	6,400

Note: The signals concerned at 4.75 ppm, 3.64 ppm, 3.38 ppm, 2.32 ppm and 0.88 ppm are corresponding to K_1/A’$_7$ (K/A’, -COC*H*NH-), T_2 (T, -O-C*H*$_2$C*H*$_2$-), T_1 (T, *CH*$_3$-*O*-), A’$_1$ (A’, -CH$_2$C*H*$_2$-CO-) and Q_1 (Q, –CH$_2$CH$_2$C*H*$_3$), respectively.

Table S4. Relative molecular weights of multifunctional PUs with different sequence orders of functional segments measured by GPC

Samples	M_n (g mol^{-1})	M_w (g mol^{-1})	$Đ$ (= M_w/M_n)
A'	5,000	5,700	1.15
8	6,900	7,400	1.07
9	7,500	8,200	1.09
10	7,200	8,000	1.11
11	6,900	7,600	1.10
12	16,300	18,900	1.16
13	17,500	20,700	1.18

Table S5. Molecular weight characteristics of various synthetic PUs

Samples	M_{n1} (g mol^{-1})[a]	M_{n2} (g mol^{-1})[b]	M_{n3} (g mol^{-1})[c]	M_{n4} (g mol^{-1})[d]	$Đ$ (= M_w/M_n)[d]
4	4,600	4,900	4,800	10,700	1.10
5	6,900	6,500	6,500	16,200	1.08
7	14,500	13,700	12,500	31,400	1.13
8	2,700	2,500	2,400	6,900	1.07
9	2,700	2,500	2,500	7,500	1.09
10	3,200	3,400	3,400	7,200	1.11
11	3,200	3,400	3,300	6,900	1.10
12	6,000	6,500	5,900	16,300	1.16
13	6,000	6,400	5,900	17,500	1.18

[a]Theoretical molecular weights from additive molecular weights of all raw segments. [b]Molecular weights calculated by integration of NMR peaks. [c]Molecular weights detected by MALDI-TOF MS. [d]Molecular weights and molecular weight distributions measured by GPC.

Note: The results of NMR and MALDI-TOF MS are in good agreement with the theoretical predictions, and the molecular weights of compounds **12** and **13** are close to each other.

Table S6. Self-assembly properties of sequence-defined multifunctional PUs

Samples	R_H (nm)[a]	R_G (nm)[a]	ρ[a]	R_D (nm)[b]	PDI[b]	ZP (mV)[b]	CAC (μg mL^{-1})[c]
KQ	73.8	53.1	0.72	153.8 ± 3.7	0.214	13.2 ± 6.4	4.45
QK	51.2	39.9	0.78	104.6 ± 2.2	0.256	-10.2 ± 3.6	3.61

[a]R_H, R_G and ρ obtained from a wide angle laser light scattering (Brookhaven Instruments BI-200SM). [b]Size (R_D), size distribution (PDI) and zeta potential (ZP) determined using a Zetasizer Nano ZS instrument (Malvern Instruments Ltd., UK). [c]Critical aggregation concentrations (CAC) acquired using a pyrene fluorescence probe technique.

Note: The micelles self-assembled from sequence-controlled multifunctional PUs (KQ: **12** and QK: **13**) exhibited a distinct difference in the surface charges.

Section 5. Supplementary References

1. N. Song, M. Ding, Z. Pan, J. Li, L. Zhou, H. Tan, Q. Fu, *Biomacromolecules,* 2013, **14**, 4407-19.

2. M. Ding, J. Li, X. Fu, J. Zhou, H. Tan, Q. Gu, Q. Fu, *Biomacromolecules,* 2009, **10**, 2857-65.

3. L. Zhou, L. Yu, M. Ding, J. Li, H. Tan, Z. Wang, Q. Fu, *Macromolecules,* 2011, **44**, 857-864.

4. A. Kowalski, A. Duda, S. Penczek, *Macromol. Rapid Comm.,* 1998, **19**, 567-572.

5. M. Ding, N. Song, X. He, J. Li, L. Zhou, H. Tan, Q. Fu and Q. Gu, *ACS nano*, 2013, **7**, 1918-1928.

6. W. Burchard, 1983, **48**, 1-124.

7. H. Liu, R. Wang, J. Wei, C. Cheng, Y. Zheng, Y. Pan, X. He, M. Ding, H. Tan and Q. Fu, *J. Am. Chem. Soc.*, 2018, **140**, 6604-6610.